



# **Preparation and characterization of polymer carrier matrices for printed wound dressings**

Master's thesis by

Sophie Rönköhharju

Pharmaceutical Sciences  
Faculty of Science and Engineering  
Åbo Akademi University  
Åbo, Finland  
2018

## Acknowledgements

I would like to thank Professor Niklas Sandler for giving me the opportunity to work on this interesting topic combining new technologies in the pharmaceutical field.

I would also like to thank my supervisor, Ph.D. Mirja Palo for all her support and encouragement and for offering invaluable advice throughout this research work.

Furthermore, I would like to thank Ph.D. Karin Kogermann for her guidance and introduction to the field of electrospinning and for all her support and contributions throughout this work.

In addition, I would like to recognize Ph.D. student Henrika Wickström for her help and all the other people involved in this project.

## Abstract

There is a vast variety of wounds that demand different therapeutic approaches for healing. Reports on real-world evidence have shown that there is a constant need for better wound dressings, as both the number of acute and chronic wounds are increasing yearly. The modern wound dressings must meet certain criteria for enhancing the wound healing process.

Wound dressings often utilize bioactive compounds such as chitosan, elastin, alginate or collagen in combination with synthetic polymers for better mechanical properties. Furthermore, different methods, such as inkjet printing, can be applied to incorporate active pharmaceutical ingredients into the wound dressings. Modern wound dressings are aimed to actively promote the healing process and provide mechanical and thermal protection for the wound, in addition to the low cost and inconvenience for the patient. Since the shape of the body parts varies extensively, it is preferable to have flexible wound dressings that are easily applied with a non-adhesive surface towards the wound. The challenge lies in finding a formulation that would be able to absorb excess fluids of the wound but retain a moist environment and promote rapid healing without having to be removed often. These requirements put high demands on the swelling ability, mechanical properties and physicochemical stability of the materials used in the wound dressings.

In this study, a bioactive compound sodium alginate was used in combination with the synthetic polymer polyvinyl alcohol to prepare wound dressing substrates by electrospinning, solvent casting, three-dimensional printing technology and the combination of them. The primary goal was to investigate the physicochemical properties and the stability of the prepared single and bi-layered substrates. Furthermore, their suitability as carrier substrates for inkjet printing of active compounds was evaluated.

Thermal crosslinking method was applied to the substrates to improve their stability in aqueous environment. Infrared spectroscopy and differential scanning calorimetry showed that the solvent cast films resulted in the most stable substrate after a storage period of one month. Additionally, the mechanical properties of all substrates were not affected by the bi-layered structure nor the crosslinking of the substrates. The substrate-ink interactions of all substrates were investigated for the incorporation of active compounds by inkjet printing. The crosslinked nanofibres exhibited low adhesion to artificial skin membrane and they seemed to be highly suitable for further functionalization by inkjet printing. Thus, this type of wound dressing substrates with a porous surface have a high potential to be used in wound care in the future.

# Contents

Acknowledgements.....	i
Abstract.....	ii
Contents .....	iii
List of abbreviations .....	v
1. Introduction.....	1
2. Literature review.....	3
2.1. Wound management.....	3
2.2. Wound dressings and their role in wound management .....	4
2.3. Materials used in wound dressings.....	6
2.3.1. Polyvinyl alcohol.....	7
2.3.2. Sodium alginate .....	8
2.4. Methods of fabrication .....	9
2.4.1. Electrospinning.....	9
2.4.2. Solvent casting.....	10
2.4.3. Three-dimensional printing .....	11
2.4.4. Inkjet printing .....	12
3. Aims.....	14
4. Materials .....	15
5. Methods.....	16
5.1. Formulation methods.....	16
5.1.1. Solvent casting.....	16
5.1.2. Electrospinning.....	16
5.1.3. Three-dimensional printing .....	16
5.1.4. Crosslinking methods .....	17
5.1.5. Inkjet printing .....	17
5.2. Characterisation.....	17
5.2.1. Texture analysis.....	17
5.2.2. Microscopy .....	18
5.2.3. Stability study.....	18
5.2.3.1. Differential scanning calorimetry .....	18
5.2.3.2. Infrared spectroscopy.....	19
5.2.4. Swelling.....	19

5.2.5. Degradation .....	20
5.2.6. Adhesion test .....	20
5.2.7. Ink characterisation.....	20
5.2.7.1. Rheology measurement.....	20
5.2.7.2. Surface tension.....	21
5.2.7.3. Jettability of ink .....	21
5.2.7.4. Ink-substrate interactions .....	21
5.3. Statistical analysis .....	22
6. Results and discussion .....	23
6.1. Physical properties of the substrates and their combinations.....	23
6.1.1. Electrospun fibres .....	23
6.1.2. Solvent cast films.....	25
6.1.3. Three-dimensional printed substrates .....	27
6.2. Puncture test .....	28
6.3. Stability of the substrates .....	30
6.3.1. Differential scanning calorimetry .....	30
6.3.2. Infrared spectroscopy .....	33
6.4. Swelling and degradation of the substrates .....	37
6.5. Adhesion of the substrates .....	41
6.6. Inkjet printing on the substrates .....	42
6.6.1. Ink properties .....	42
6.6.2. Contact angle .....	43
6.6.3. Inkjet printing trial.....	45
7. Conclusions.....	49
8. Swedish summary (svensk sammanfattning).....	51
9. References.....	55

## List of abbreviations

.stl – stereolithography (file)

2D – two dimensional

3D – three dimensional

BB – 3D printed substrate

CAD – computer aided design

DDS – drug delivery system

DSC – differential scanning calorimetry

ECM – extracellular matrix

IR – infrared spectroscopy

NF – nanofibres

PBS – phosphate-buffered saline

PG – propylene glycol

PVA – polyvinyl alcohol

PM – physical mixture

SA – sodium alginate

SEM – scanning electron microscopy

SC – solvent casting

SCBB – solvent cast/3D printed substrate

SCNF – solvent cast/nanofibre substrate

$T_g$  – glass transition temperature

$T_m$  – melting temperature

UV – ultraviolet

# 1. Introduction

There are many different wound types that target various aspects of the wound healing process. An ideal dressing should provide enhanced healing with minimal inconvenience at low cost for the patient [1]. Traditional wound healing agents involve topical liquid and semi-solid formulations along with traditional dry dressings from synthetic or organic materials [2]. New emerging technologies, such as tissue engineering and the use of novel materials and biopolymers, have been introduced to the market to reach improved wound healing. The fundamental characteristics of modern wound dressings are to maintain and generate a moist environment around the wound and to promote wound healing [3].

Most novel dressings are made from polymers that can act as carriers for delivery and release of drugs to the wound site. Some of the polymers used in novel wound dressings are alginates, hydrogels, hydrocolloids, polyurethane, collagen, chitosan, pectin and hyaluronic acid [4][3]. In addition, some formulations have pharmacological agents incorporated, such as antibiotics, vitamins, minerals, growth factors and other wound healing accelerators that function as an active part in the healing process [3]. The delivery of antibiotics to local wound sites is the most preferred option over systemic administration to decrease the risk for incompatibilities. Modern wound dressings need to deal with differences in the characteristics of wounds such as fluid retention, adherence and dressing residues to reduce the occurrence of skin maceration caused by excessive wound exudates [4]. Furthermore, they need to possess suitable physical and mechanical properties, such as tensile strength, bioadhesion, rheological properties (gels and films) and/or appropriate sustainability to compression [2][3]. Characterizing the mechanical properties of wound dressings is important since film dressings need to be durable, stress resistant, soft, flexible, pliable and elastic to be able to withstand the stresses exerted by different parts of the body [3]. Moreover, they should be easy to apply and remove without causing any trauma or damage to the new sensitive epithelial layer when changing the dressing.

The formulation development is reaching towards obtaining optimal physical properties and controlled delivery characteristics for active wound healing dosage forms. Incontrovertibly, the ideal composite dressings should combine the different characteristics of current wound dressing technologies. This would facilitate the targeting of many features of the complex wound healing process, to guarantee effective, complete wound healing and faster healing

for chronic and/or severe wounds. Utilizing individualised therapeutic approaches could also prove helpful for treating certain wound types and individuals.

In this study, a combination of a synthetic polymer and a biological compound was used to find a suitable formulation for wound dressing applications. The polymer substrates were prepared with emerging tissue engineering technologies through the aid of electrospinning, three-dimensional (3D) printing and solvent casting techniques. The mechanical and physicochemical properties of the substrates were evaluated. Furthermore, the suitability of the substrates for inkjet printing was investigated for the incorporation of drugs into the wound dressings in the future.



## 2. Literature review

The skin is the largest organ of the human body and accounts for many different functions [5]. Millions of people every year suffer from accidents caused by flames, hot water, and boiling oil, that lead to major disabilities or even death [6]. Reports from real-world evidence have highlighted the substantial burden that acute and chronic wounds impose on the health care units [7]. The frequently increasing comorbidities cause more wounds that are more difficult to treat and therefore there is a huge need for more effective wound dressing on the market.

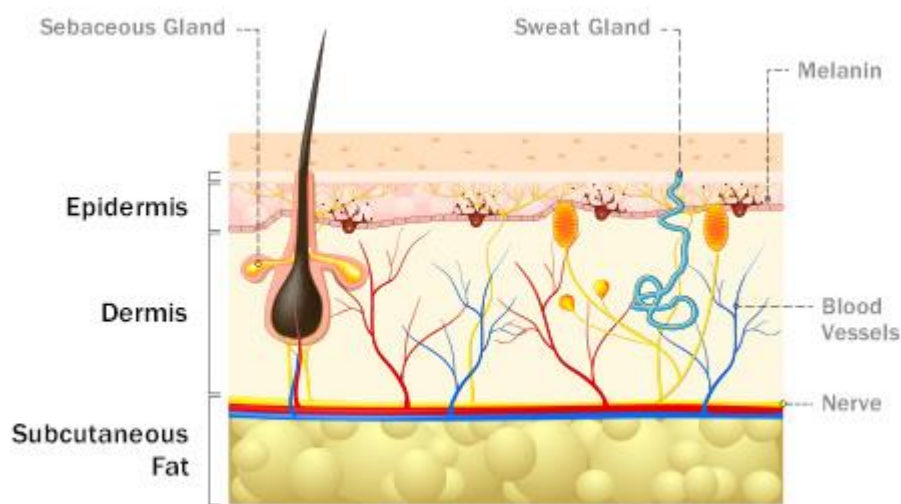
### 2.1. Wound management

To achieve effective wound management, it is necessary to understand the different factors affecting it. The wound type, healing process, environment, medical conditions (e.g. diabetes), and social setting are the factors that mainly determine the treatment of the wounds [3]. The definition of a wound is the result of ‘disruption of normal anatomic structure and function’ according to the Wound Healing Society as cited by Boateng *et al.* [3]. It can be caused by an underlying medical or physiological condition and can derive from either a physical, thermal or chemical damage.

Wounds can also be divided into two classes based on the repair process: acute and chronic wounds. Acute wounds are small and heal completely with minimal scarring within 8-12 weeks. Chronic wounds take longer than 12 weeks to repair and often reoccur. They are usually caused by some underlying disease, persistent infection or by poor primary care of the wound [3]. The healing process of a wound progresses in three stages. The bleeding occurs almost immediately to flush out bacteria and foreign object, followed by the inflammation that causes vasodilatation through the release of serotonin and histamine. This phase usually takes up to three days, after which endothelial cells, keratinocytes, dendritic cells, and fibroblasts are activated for replacing the damaged and lost tissue. This is also when the immune system steps in and recruits neutrophils, monocytes, and lymphocytes for dealing with inflammatory agents [1][3]. The final steps of the healing take place from the third day onwards as basal cells proliferate granulated tissue, and capillaries and lymphatic vessels grow into the wound simultaneously. The connective tissue is formed that strengthens the new epithelium and determines the nature of the final scar. The extracellular matrix (ECM) provides the physical support needed for the cells as they organize themselves and secrete the components needed for tissue regrowth [1]. Moreover, the exudate secreted

from a wound during the healing provides the wound with nutrients, favourable conditions for tissue growth and leucocytes to help with controlling bacterial infections at the wound surface [3].

To fully understand the process of tissue regeneration it is important to know the basic elements constituting the skin (*Figure 1*). The outmost layer of the skin is called epidermis. It is waterproof and is responsible for protecting the body against damaging environmental factors. It is composed of mostly dead cells, a protein called keratin, blood vessels, and nerves [5]. The middle layer is called dermis and is composed of living cells. The subcutaneous fat layer accounts for the insulation and shock absorbance. When the top layers of epidermis are shed off, the cells on the surface are being replaced by new skin tissue constantly from below. However, the regeneration of dermis cannot occur spontaneously for neither adults nor elderly people [6]. Because of this, there is a limit to the regenerative ability of autologous skin and it is closely related with additional scarring. When substantial loss of the outer layers occurs, dressing materials become inevitable for skin tissue replacement or healing.



*Figure 1. Schematic representation of the skin and its structure [8].*

## 2.2. Wound dressings and their role in wound management

In the attempt of developing novel substrates for wound healing there is a need for robust, non-toxic, bioadhesive and mechanically stable carrier substrates. There are several different kinds of wound dressings available on the market for the treatment of different types of

wounds. Since 1960s and the utilization of mainly natural dry materials, wound dressing development has gone far. Nowadays, novel wound dressings are made from combinations of polymeric materials and play an active role in the healing process [9]. Wound dressings can be classified according to their role in the wound healing process [2]. Passive products are ordinary dressings, such as gauze or tulle, which only acts as a cover that the wound can rehabilitate underneath. The second types of wound dressings are interactive materials made from polymeric films and/or foams that are transparent and permeable to water vapor and oxygen. The polymers, such as hyaluronic acid, hydrogels or foamed covers, act as barriers against bacteria entering the wound environment. The third types of wound dressings are bioactive materials made from biological materials such as alginates, collagens, chitosan, and hydrocolloids. Functionalized biomaterial dressings enhance the healing since they last longer before needed to be changed and have the ability to modify the chemical environment of the wound area in favour of accelerated wound healing. Ideally, a wound dressing should maintain a local moist environment, prevent infection and mechanical trauma, provide thermal insulation, absorb wound fluids and exudates but prevent dryness and necrosis, stimulate the growth rate and be elastic, non-toxic, non-antigenic, non-allergenic, biocompatible and biodegradable [2][9]. Furthermore, they should cause minimal inconvenience for the patient by providing rapid healing at an acceptable cost, absorbing any wound odours, being non-adherent to the wound and easy to remove without causing trauma to the wound [1][2]. Sufficient oxygen supply to the tissue is another important factor to take into account. This is partly taken care of by the body itself through incremental angiogenesis during the healing process, but the wound dressing should also strive to have a good oxygen transmission capacity to achieve an optimum healing process [1][2][3].

Even if the restoration of tissue after an injury is a natural phenomenon, there are many factors that can complicate and slow down the process of healing. If an open wound is exposed to air directly it will dehydrate and a scab or scar will form [5]. The mechanical barrier that is formed is blocking the dermal cells from migrating outwards and they are forced to move into a deeper level of tissue. This prolongs the healing process. Other than that, the infection can complicate the healing process. In other words, a moist environment is more ideal for a faster wound healing process as this prevents the formation of scab. Traditionally, the management of wounds has been focusing on keeping the wound dry by using different kinds of natural and synthetic bandages, cotton wool, lint and gauzes [2][3]. This is correct in the sense that the primary function of a wound dressing is to keep the

wound protected from harmful bacteria (that thrives in moist environment), but contradicts the fact that a warm, moist wound environment has been proven most beneficial for rapid and successful wound healing. Junker *et al.* [10] found that a wet or moist wound treatment significantly reduces the time required for re-epithelialization, and that it leads to reduced inflammation, necrosis, and subsequent scar formation. Furthermore, they also concluded that it has no adverse effects on the wound itself or the surrounding tissue. Many modern wound dressings take model after the natural exudate of the body and utilize the concept for maintaining moisture at the wound bed but also removing excess exudate from the wound. This is no easy task, as the amount and production rate of exudate varies from time to time and between different wound types. If the absorptive capacity of the dressing does not correlate with the exudate production rate the maceration of the skin surrounding a wound can occur [4]. This happens if there is an excess of exudate present for a longer period of time in an occlusion on the wound. However, if the dressing is highly absorptive, it might need more frequent dressing changes to investigate and manage the cause of the exudate (such as infection), and to prevent necrosis formation in the case of excessive drying.

### 2.3. Materials used in wound dressings

The wound dressings of today are classified according to the materials from which they are produced. These includes hydrocolloids, alginates and hydrogels, and exist in the form of gels, thin films, foam sheets and fibres [3][4]. Hydrocolloids are a group of wound management products from gelling agents (colloids) that are combined with other materials such as elastomers and adhesives. Typical gelling agents are (sodium) carboxymethylcellulose, gelatine and pectin that in many cases are bonded to semipermeable film or foam sheet carriers to produce flat and occlusive adhesive dressings [4]. Alginate dressings are another type of dressings that also form gels, but through a different method that is explained in detail later. They occur in the form of freeze-dried porous sheets (foams) or as flexible fibres. Hydrogels are mostly made from synthetic materials such as poly(methacrylate) and polyvinylpyrrolidone that form insoluble and swellable hydrophilic dressings. Nylon and its derivatives were originally used together with polyethylene and polyurethane for film dressings. Today most of the sterile plastic sheet products available are made from polyurethane coated with hypoallergenic acrylic adhesives as primary wound cover [4]. Polyurethane can also form porous foams that are used together with adhesive borders. Some foam dressings are also made from silicone.

The latest development in wound dressings are bioactive dressings. These are made from biomaterials that have an active role in the wound healing process and are often produced with tissue engineering. Most technologies combine different polymers such as collagen, hyaluronic acid, chitosan, alginate or elastin [3]. Additional component such as antimicrobials, growth factors or different supplements can also be added to the dressings to achieve more rapid wound healing.

Poor nutritional status or old age are factors that can affect the ability to heal a wound and fight an infection [3]. The deficiency of proteins, vitamins (E, C and A) and minerals impede the inflammatory phase which prolongs the healing time of the wound. Anemia and diabetes are underlying diseases that can affect the wound healing process gravely. In these cases, it is important to understand the cause behind the impairment of the wound healing process and to have dressings with specific characteristics available for treating certain wounds. A wet environment, such as one provided by hydrogels and wound environment, can allow for precise delivery of antimicrobial agents (i.e. antibiotics or ZnO) and analgesics to the wound area [10][11][12]. Other bioactive molecules such as growth factors can also be introduced in a controlled manner in a wet wound-healing environment [10]. The introduction of drug components or other bioactive molecules have beneficial effects on the wound healing process and can allow for longer time periods between change of dressing or accelerate the healing speed of a wound.

In this thesis, a combination of synthetic and natural materials was used. The properties of these polymers are described below in more detail.

### 2.3.1. Polyvinyl alcohol

One of the most frequently used and early synthesized synthetic polymer in hydrogels is polyvinyl alcohol (PVA) [9]. PVA is an easily film-forming agent of excellent biocompatibility and has been applied in several biomedical applications such as soft contact lenses, reconstructive joints, wound dressings and drug delivery applications [13][14][15][16]. Furthermore, it is water-soluble, biodegradable, non-carcinogenic, bioadhesive, and easily processable. Because of this, PVA is able to mimic natural tissues that can be accepted into the body. Hydrogels form a network of hydrophilic polymers that can swell and hold water in large amounts whilst maintaining their structures [17].

Crosslinking of the polymer chains enables the formation of this network and the gels are called permanent or chemical gels when they are covalently crosslinked [14]. This can be

provided through hydrogen bonding, van der Waals interactions or physical entanglements. Both chemical and physical crosslinking methods such as freeze-thawing, heating, irradiation, aldehyde treatment and radical production have been tested for PVA [18]. Although PVA easily forms a hydrogel, the properties of the produced film are mechanically not good due to rigidity and stiffness [19]. PVA has previously been mixed with natural or synthetic polymers to improve the mechanical and physiochemical properties of the films. Dextrans, glucans, alginate, chitosan, gelatine, starch, cellulose are examples of natural polymers that have been used together with PVA in different wound dressing applications [20][21][22][23].

### 2.3.2. Sodium alginate

Sodium alginate (SA) is natural polymer often combined with PVA in wound dressing composites due to its excellent swelling abilities [4][9]. It is obtained by extraction from brown algae and composes of anionic linear polysaccharide polymers with a varying ratio of random or alternating 1,4-linked  $\beta$ -D-mannuronic acid (mannuronate) residues and 1,4-linked  $\alpha$ -L guluronic acid residues [9]. Alginate is a highly hydrophilic, biocompatible and relatively low-cost polymer that has been used in various wound treatments and other pharmaceutical applications earlier [11][12][24]. Alginates can absorb 15-20 times their own weight of fluid, which impacts greatly on the moisture management of the wound [4]. The swelling also lowers the adhesion between the wound and the wound dressing, thus causing less trauma to the newly formed tissue upon removal of the dressing.

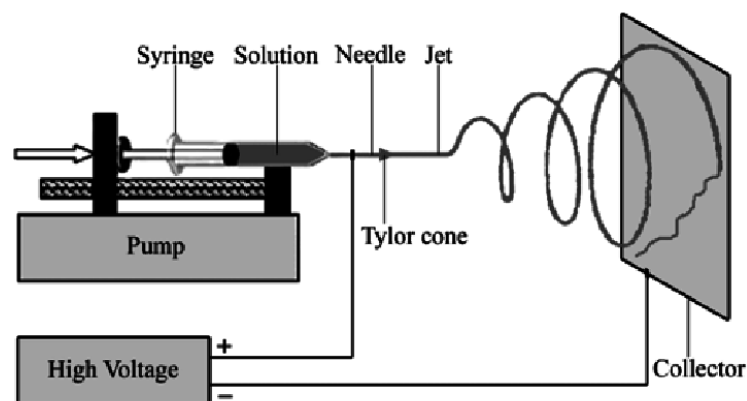
The formation of a soluble alginate gel happens as the calcium from the wound's exudate and sodium from the alginate undergo an ion exchange [24]. Monovalent metal ions (such as  $\text{Na}^+$ ) form soluble salts with alginate, whereas divalent and multivalent cations (i.e.  $\text{Ca}^{2+}$ , except  $\text{Mg}^{2+}$ ) form gels or precipitates [24]. Different cations have a different affinity for alginate, and the selective ion binding is the fundamental element for the ability of alginate to form ionotropic hydrogels. Alginates with a low content of mannuronate give gels lower strength compared to alginates rich in guluronic acid blocks, as guluronic acid residues exhibit a stronger affinity for divalent ions than the mannuronate residues. According to Kim *et al.* [12], SA also increases the thermal stability and the mechanical properties of the hydrogel film when added to PVA [12]. The same study also showed that SA is inert towards the release profile of clindamycin. This means that alginate has desirable properties for drug loading as well.

## 2.4. Methods of fabrication

Traditional wound treatment formulations include topical liquid (solutions) and semi-solid (ointments/creams) formulations in addition to dry dressings [3]. The liquids are effective in the initial stages of wound healing for cleaning of the wound and reducing the bacterial load. Dry dressings are used directly on the wound or form part of a composite of several dressings, where each part performs a specific function. Traditional dry dressings are made from woven and nonwoven fibres of cotton, polymers or a combination of both. Modern dressings are primarily classified according to the materials they are made from including hydrocolloids, alginates, collagens, hydrofibres and hydrogels [2][3]. These generally occur in the form of gels, foam sheets, nonwoven pads or thin films. Modern fabrication methods such as electrospinning and printing technologies provide products with unique properties for the application of these materials on many different wound types. The methods used for preparing the substrates in this work are described below in more detail.

### 2.4.1. Electrospinning

Electrospinning is a mean of producing a nonwoven, three-dimensional (3D) nanoscale fibre-based matrices. The electrospinning process was introduced the first time in the early 1930s and has been continuously investigated ever since [25]. The process can be seen in *Figure 2* and it includes a syringe filled with polymer solution, to which a pump and a power source with high voltage is applied to overcome the surface tension of the solution [26]. The polymer jet is drawn by combining the force of gravity with mechanical pumping and electrostatic charge. Evaporation of the solvent mid-air creates higher surface charge density and nanofibres are formed as the ejected jet undergoes narrowing. The fibres are collected onto a stationary plate or rotating collector depending on the wanted alignment of the fibres.



*Figure 2. Schematic representation of the electrospinning method [27].*

Electrospinning has many applications in the biomedical field such as drug release formulations, enzyme immobilization, tissue engineering and wound dressings [28], the latter being the final intended application of this study. Nanofibres are especially of interest for wound dressings since they have a high porosity (that can be altered by the electrospinning process), beneficial size scale and topography, high surface area to volume ratio, high oxygen transmission capability and allow absorption of excess exudates [29][30]. The fibres are also capable of mimicking the ECM which is important for the wound healing process and more porous fibres are considered more suitable as scaffolds for cell populations than dense fibres as the porous structure actively promotes the cell attachment [30][31]. As the fibres in this study are made from biocompatible polymers such as SA and PVA, their potential use as substrates in wound dressing application as well as printing substrates is promising [25]. Polymers used in electrospinning have been reported to be either synthetic, natural or combinations of the two [32]. Electrospinning of natural polymers is not always possible due to inherent properties, but the addition of certain polymers offers the enhancement of the properties of polymeric materials and also lowers the basic cost. Property enhancement includes tailoring of thermal stability, mechanical strength and processability [32][33]. Specific intermolecular interactions, formed through hydrogen bonding between two or more polymers, lead to enhanced electrospinning performance when the blends are prepared from aqueous solutions [33].

#### 2.4.2. Solvent casting

Solvent casting is an easy way of creating polymeric films that could be used as polymer carrier matrices for wound dressings. The films are prepared by dissolving a film forming polymer (e.g. hydrophilic polymers) in a solvent and pouring the solution onto a flat surface [34]. When the solvent has evaporated, a thin polymer network film is created that can be cut into strips of wanted size [34][35]. Due to the simplicity of the method and the affordability of the equipment it is preferred by the pharmacies for small scale preparations [36]. However, the method is proved to be somewhat problematic when a drug is incorporated in the solution used for solvent casting [35]. Unwanted events such as crystallization may occur during storage due to the super-saturated concentration of the drug after the solvent has been removed from the film [34][35].

The polymers used in solvent cast films for biological application need to be soluble in volatile solvents or water. Furthermore, they need to be stable in solution with a minimum content and viscosity and they should form a homogenous film that releases easily from the



casting support material [37]. The films should be easy to handle, flexible, somewhat elastic, and soft but possess enough strength to endure mechanical stress during manufacturing, distribution, and final handling by the patient [34][35]. Apart from polymeric components, plasticizers can be added to achieve different properties but also the ratio of polymers, manufacturing process, process techniques (co-solvent systems, dissolution at over-pressure, special molecular weight distributions of polymers or co-polymers, release agents etc.), storage conditions and additives can affect the properties of the film (thickness, elasticity, anti-static/-blocking properties, transparency, conductivity etc.) [34][37]. When the technology was developed around 40 years ago cellulose derivatives were mostly used together with water. Water is still today a common solvent in food-graded films made from biopolymers or PVA [37]. The immediate advantages with solvent cast film on an industrial scale are that they are easy to make, have a homogenous thickness distribution, high optical purity, excellent transparency, are thermally or mechanically possible to process and have high-temperature resistant from non-melting but soluble raw materials. The disadvantages are the high production cost due to the dependence on slow solvent diffusion process and extra solvent recovery or the investments in the facilities for handling solvents and dope solutions [37].

#### 2.4.3. Three-dimensional printing

3D printing is another flexible method that brings basically any design to reality and it is extremely useful in many different areas including the pharmaceutical one. In this specific field, the technology can be used to create personalized dosage forms but also medical devices and engineered tissue [38][39]. 3D pharming is a term used for the various 3D and two-dimensional (2D) printing techniques in the purpose of producing patient specific formulations in a manner of speed and precision [39]. The prototype of the design is made by the help of computer aided design (CAD) programs, which is then exported into a rapid prototyping stereolithography (.stl)-file format [40]. The file originating from the CAD program gives the geometrical shape and size of the prototype, but the .stl-file generates the coordinates of triangles that collectively form the surface of the designed 3D model. The printing device subjects the .stl-file to a series of actions to receive a sliced 3D model composed of several layers. Once the first layer is deposited, the rest of the layers are subsequently printed on top of it. The 3D model in the computer program is accordingly reduced by the thickness of each next layer until the whole design is finished. Each layer must solidify for the desired structure to be completed. 3D pharming is a refined way of

designing well-structured, accurate and tailored drug delivery systems (DDS) from inexpensive materials, which can be installed and operated in various environments, including health care facilities if provided with the correct input material [39][40]. However, there is a need for standardized validation methods of designing, printing and post printing, as well as physical and mechanical assessments of the final devices [41]. The convenience and readily available printed structures, however puts pressure on the development of a standardized validation method for the evaluation of sterility, cleaning, and biocompatibility of the final product. The benefits of 3D printing lie in the highly scalable and cost effective production, the possibility to print both the support material and multiple drugs together in very precise amounts (that also are trackable), which offers a remarkable access to quality assurance [39][41].

#### 2.4.4. Inkjet printing

Inkjet printing is a technique which has been used in the field of diagnostics, medical sciences and genetics, in attempts of incorporating drug substances, or even DNA, in or on top of the final application [41]. Inkjet printing is an excellent non-contact approach for applying drug layers on top of different materials with the aid of computerized design [41][42] (*Figure 3*).

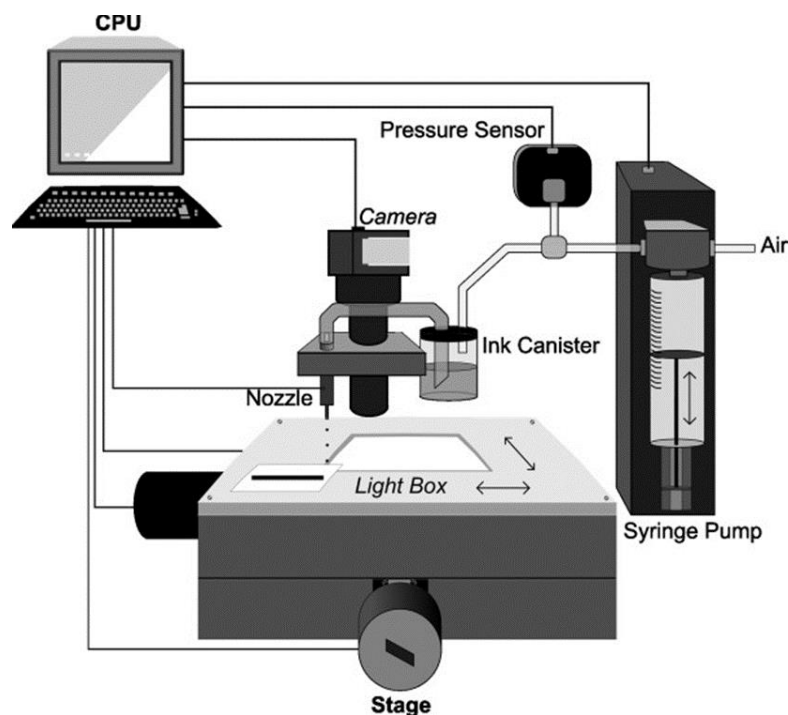


Figure 3. Schematic representation of inkjet printing technology [43].

The technological aspects for the technique were invented already in the 1950s but it was mostly used for simple marking of materials during that period [44]. More recent application areas are e.g. microstructure patterning [45], electronic components [46], ceramic components [47], biosensors [48] and tissue engineering [49]. The IJP technique produces droplets with a diameter range of 10 to 150  $\mu\text{m}$  that are printed into 2D or 3D structures. Single droplets are formed under pressure, created by either i) heating of the liquid up to a temperature greater than the boiling temperature or ii) by applying voltage (1-60 kV) to a piezoelectric transducer that generates vibrational waves in the material [44]. The material of interest must be dissolved or dispersed in a liquid to form a printable ink. The inkjet printing technique is an attractive fabrication method for DDS since it enables easy control over the model drug release profile, where parameters such as the release rate and release time can be controlled by altering the microstructure, composition or location of the model drug within the matrix [42].

### 3. Aims

The current strategies and medical products for wound healing are often insufficient for effective treatment. Thus, there is a need for advanced wound care products such as wound dressings with more flexible and interactive substrates. The main aim of this study was to develop and investigate novel polymer formulations as a biocompatible and bioadhesive wound dressing. These formulations were aimed to be used in printed wound dressings, where inkjet printing could be used as a flexible and convenient method to introduce active compounds into the wound dressings.

The specific aims of the study were to:

- Prepare single- and bi-layered wound substrates by combining different methods
- Characterize physicochemical and mechanical properties of the wound substrates
- Investigate the surface properties of the substrates related to bioadhesion and printability
- Evaluate the suitability of the substrates to be used for inkjet printing of refined wound dressings

## 4. Materials

The solutions used in the experiments were made from polyvinyl alcohol (PVA, Mowiol® 20-98,  $M_w$  125,000 g/mol, Sigma-Aldrich Chemistry, Germany) and sodium alginate (SA, Sigma-Aldrich, Norway) in different concentrations keeping the weight ratio between the two ingredients constant. PVA was dissolved in water at 85 °C for about 2-3 h while stirring, once dissolved the solution was left stirring overnight at room temperature (RT, 20±5 °C). SA was dissolved in water at RT while stirring and left stirring overnight. The two solutions were mixed in 80:20 volume ratio in different concentrations. The solution A that consisted of PVA 12 and SA 2% in 80:20 ratio was used in the solvent cast method. The solution B that consisted of PVA 18% and SA 3 % in 80:20 ratio was used for the printed substrates. A physical mixture (PM) of PVA and SA was prepared with the same ratio as in the solutions of the polymer mixtures. The particle size of PVA was reduced by grinding with mortar and pestle.

The samples in the swelling and the degradation study were kept in 10 ml phosphate-buffered saline (PBS) solution (BioWhittaker® PBS, Lonza, Belgium) and in-house made PBS-solution made from  $\text{HNa}_2\text{O}_4\text{P}$  (Fluka Analytical, Germany),  $\text{KH}_2\text{PO}_4$  (Emsure®, Merck KGaA, Germany), NaCl (Sigma-Aldrich, USA) with pH 7.4±0.1.

The ink base used in the inkjet printing was made from propylene glycol (PG, Sigma-Aldrich, lot#MKBX0067V, USA) and purified water with a concentration of 40% (PG40). The final ink solution was coloured with red food colour (Dr. Oetker Sverige AB, Sweden). Prior to printing, a test series of solutions with PG in concentrations of 10-90% (labelled as PG10-PG90, accordingly) was analysed.

An artificial wound fluid was made in-house for the adhesion test [50]. It contained 2% bovine serum albumin (Sigma-Aldrich, USA), 0.02 M  $\text{CaCl}_2 \cdot 2\text{H}_2\text{O}$  (MERCK, Germany), 0.4 M NaCl (Sigma-Aldrich, USA), 0.08 M Tris(hydroxymethyl)-aminomethane (MERCK, Germany) and purified water.

## 5. Methods

### 5.1. Formulation methods

#### 5.1.1. Solvent casting

Solvent cast (SC) substrates were prepared as films that were cast on top of commercial copier film (Folex<sup>®</sup>IMAGING, X-10.0, Germany) or aluminium foil by pouring solution A onto the copier film and levelling it with a film applicator (Multicator 411, Germany) set at a wet height of 500 and 1000  $\mu\text{m}$ . The films were lightly covered to prevent dusting and dried for 2 days at ambient conditions (RT and relative humidity (RH) of  $20\pm 5\%$ ). The final films were stored in the refrigerator throughout the study.

#### 5.1.2. Electrospinning

The electrospinning was carried out at University of Tartu, Estonia. The nanofibrous (NF) substrates were prepared using the eS-robot<sup>®</sup> (NanoNC, ESR-200Rseries, South Korea) electrospinning machine. The electrospinning was conducted at  $25.4\pm 0.4$  °C and RH of  $17.5\pm 0.5\%$ . The spinning parameters were optimized for the polymer solution (solution A) with a voltage of  $11\pm 1$  kV and 0.3 ml/h flow rate generating a fibre mat of approximately  $24\times 20$  cm from 8 ml solution. A single syringe with a 23 G needle tip was used to eject the solution onto a rotating (25 rpm) metal collector covered in aluminium foil at a distance of 15 cm from the tip of the needle to the collector.

Bi-layered solvent cast/nanofibre (SCNF) substrates were prepared onto SC films (cast on aluminium foil) by electrospinning with the same method mentioned above.

#### 5.1.3. Three-dimensional printing

Solution B was used to print  $1.65\times 1.65$  cm single-layered squares with Biobots 1 semi-solid extrusion type three-dimensional (3D) printer (BioBots Inc, USA, currently known as Allevi). Films with a grid-like pattern were prepared to achieve a more porous structure. The prototype (.*stl*-file) of the square was designed using the computer-aided design FreeCAD<sup>®</sup> program (0.16, 2001-2015). The 3D design was sliced (.*gcode*-file) using Repetier-Host software (V1.6.1, Hot-World GmbH & Co. KG, Germany). The substrates were printed with a 25 G needle as one layer (wet height: 0.15 mm) in a 40% honeycomb infill pattern with 3 perimeters, creating a grid with macropores across the square. The printing was performed at a pressure of 60-70 psi with a printing speed of 4 mm/s. The 3D printed (BB) substrates

were printed on commercial copier films and thus created a porous structure once dried and removed from the copier film.

The solvent cast/3D printed (SCBB) substrates were printed on top of the SC films, creating a bi-layered structure.

#### 5.1.4. Crosslinking methods

Crosslinking is a necessary means to make the substrates more stable in an aqueous environment (i.e. wound environment). In this study, thermal and UV (ultraviolet) crosslinking methods were used. The thermal crosslinking was performed at 180 °C in an oven (Memmert, DIN 12880-KI.1, Germany) for 10 min. The UV crosslinking was performed with a LED flashlight (365 nm, MTE<sup>®</sup> UVA 303, Singapore) at a distance of 7 cm from the flashlight to the sample for 10 min. After the initial studies, the UV crosslinking method was discarded due to its insufficiency in making the substrate water durable; therefore, further studies were continued with thermally crosslinked substrates.

#### 5.1.5. Inkjet printing

The suitability of the substrates for inkjet printing was tested on both non-crosslinked and thermally crosslinked SC, SCBB and SCNF samples. A PG40 solution with 9.1% red food colour was used as ink. The ink was printed with a PixDro LP50 piezoelectric inkjet printer (Meyer Burger Technology Ltd, Switzerland) in 2×2 cm squares with 450 and 100 dpi. The printing parameters were as follows: bidirectional print direction, ink pressure of -21 mbar, and voltage of 100 V. Using a nozzle diameter of 50 µm the droplet size was approximately 45 pl.

### 5.2. Characterisation

#### 5.2.1. Texture analysis

A puncture test was carried out to measure the mechanical strength of the substrates, using Texture Analyser TA.XT*plus* (Stable Micro Systems, Surrey, UK) equipped with a film support rig (HDP/FSR) and a spherical stainless steel probe ( $\varnothing=5$  mm, P/5 S). A digital calliper (Mitutoyo, 500-171-21, CD-6", Japan) was used for thickness measurement. The measurements were performed with a pre-test speed of 2 mm/s, test speed of 1 mm/s and a post-test speed of 10 mm/s. The maximum force (N) needed to break the substrates was recorded (break force).

An initial testing of the SC films was carried out to determine a suitable thickness for the SC substrates. Films cast from solution A with wet height of 500 and 1000  $\mu\text{m}$ , as well as films from solution B with the same wet height for casting were analysed (n=20). Thereafter, the measurements were performed with all the prepared substrates (SC, BB, NF, SCBB, SCNF) (n=10).

### 5.2.2. Microscopy

The printed samples were visualized with a digital microscope (ProScope, Bodelin Technologies, PSEDU-100, OR-USA). Scanning electron microscope (SEM, Leo Gemini 1530, Zeiss<sup>®</sup>, Germany) equipped with secondary electron and In-Lens detectors was used for visualizing the SCBB and SCNF substrates in the original state and after the degradation study, and the inkjet printed samples. The substrates were sputter-coated with carbon using a vacuum evaporator. The fibre morphology of the NF samples was visualized with EVO MA 15 (Zeiss<sup>®</sup>, Germany). The NF samples were magnetron-sputter coated with a 3 nm gold layer in an argon atmosphere prior to microscopy image acquisition. The SEM and microscopy images were analysed with ImageJ (1.51j8, National Institute of Health, USA) to depict fibre morphology and diameter measurements. The infill percentage of the BB sample surface was checked with ImageJ.

### 5.2.3. Stability study

A stability study was performed according to EMA guidelines [51] with non-crosslinked and crosslinked samples, made from electrospinning and solvent cast method. The crosslinking methods included were UV and thermal crosslinking. The samples were stored for one month in desiccators in two separate conditions: i) elevated temperature (40 °C) and humidity (RH of 75%), and ii) RT and low humidity (RH of 0%). The physiochemical properties of the samples were measured with differential scanning calorimeter (DSC), infrared (IR) spectroscope after 24 h, 1 week and 1 month in addition to the initial state of the samples (0 h). Information about the temperature and humidity was collected with USB Datalogger (WK057 Version 2.0, Wisemann Klein, Spain).

#### 5.2.3.1. Differential scanning calorimetry

DSC measurements were done to compare the water content and detect changes in the physical properties of the substrates during the stability study. One substrate from each timepoint at each condition was analysed with Pyris Diamond DSC (PerkinElmer Instruments, USA). Samples of 1-3 mg were placed into 30  $\mu\text{l}$  aluminium pans with pierced



lids. The heating rate of the samples was 10 °C/min with 25 °C as a starting point and 250 °C as an ending point. A N<sub>2</sub> purge with a flow rate of 40 ml/min was used in the oven. The DSC system was calibrated using indium (156.6 °C). Thermograms were baseline corrected prior to analysis.

#### 5.2.3.2. Infrared spectroscopy

The substrates from the stability study were measured after 24 h, 1 week and 1 month using a universal attenuated total reflectance Fourier transform IR spectroscope (UATR Two, Perkin Elmer, UK). The measurements were conducted in a spectral range from 450 to 4000 cm<sup>-1</sup> with 4 scans per measurement (n=3). A PM of SA and PVA in a corresponding ratio to the prepared solutions as well as powders of the two substances separately were measured as reference. The data collection and the pre-treatment of the IR spectra with baseline correction and smoothening by a factor of 30 was done with Spectrum 10.03 software (PerkinElmer, UK).

#### 5.2.4. Swelling

A swelling study was conducted to test the stabilization performance of the crosslinking method and the stability of the substrates. The single-layered (SC, NF, BB) and bi-layered (SCNF, SCBB) substrates were included in the study. Both thermally crosslinked and non-crosslinked substrates were included. The samples consisted of cut squares with a size of approximately 1.65×1.65 cm.

The samples were weighed and then immersed in 10 ml of PBS solution in 50 ml Falcon<sup>®</sup> tubes. The samples were mixed (30 rpm) at 37 °C in a water bath (Sotax AT7, Switzerland) for 24 h, 3 days and 7 days. The mass of the SC, BB, SCBB and SCNF samples was weighed with a microbalance (d=1 µg, MYA 2.4Y, Radwag Wagi Elektronicze, Poland), and the mass of the NF samples was weighed with an analytical balance (APX-200 balance, Denver Instruments, U.S.). The samples were weighted after excess fluid had been removed from the swollen sample with filter paper immediately after taking the samples out of the PBS solution. The samples were then dried for 7 days under a ventilated fume hood after which they were weighed again. The swelling study was conducted in triplicate.

The swelling ratio was calculate using *Equation 1* [52]:

$$\text{Swelling ratio } \left(\frac{g}{g}\right) = \frac{w_s - w_0}{w_0}, \quad (1)$$

Where W<sub>s</sub> is the swollen sample and W<sub>0</sub> is the initial sample weight.

### 5.2.5. Degradation

The same set of substrates used in the swelling study was used in the degradation study. The substrates were immersed in 10 ml of PBS solution in 50 ml Falcon<sup>®</sup> tubes at 37 °C in a water bath for 24 h, 3 and 7 days. The substrates were weighed before immersion, after removal from the water bath, and after being dried for 7 days under a ventilated fume hood. The degradation study was conducted in triplicate. The weight loss percentages were calculated using *Equation 2* [52]:

$$\text{Weight loss (\%)} = \frac{w_0 - w_1}{w_0} \times 100, \quad (2)$$

Where  $W_0$  is the initial weight of the sample and  $W_1$  is the dry weight of the sample obtained after PBS immersion.

### 5.2.6. Adhesion test

The adhesion of the crosslinked and non-crosslinked substrates (SC, NF, BB, SCNF, SCBB) to artificial skin (VitroSkin<sup>®</sup> N-19, IMS Inc., Lot#7360, USA) was tested with Texture Analyser TA.XTplus (Stable Micro Systems, Surrey, UK) equipped with a mucoadhesion rig (A/MUC) and a cylinder delrin<sup>®</sup> probe ( $\varnothing=10$  mm, P/10). The adhesion test was performed according to a slightly modified method presented previously by Tamm et al. [53]. In brief, circular shaped samples of the substrate ( $\varnothing=11$  mm) were prepared with a hollow punch and attached to the probe with Scotch<sup>™</sup> adhesive double-sided tape (3M, USA). An aliquot (200  $\mu$ l/sample) of artificial wound fluid was pipetted on the artificial skin before the measurement. The testing conditions were set as follows: pre-test speed 0.5 mm/s, test speed 0.5 mm/s, post-test speed 5 mm/s, applied force 1 N, return distance 100 mm, contact time 60 s, and trigger force 0.05 N. Scotch<sup>™</sup> adhesive double-sided tape, and DuoDERM<sup>™</sup> (ConvaTec Inc., UK) and Aquacel<sup>™</sup> (ConvaTec Inc., UK) commercial wound dressings were used as references. All experiments (n=6) were conducted at ambient conditions.

### 5.2.7. Ink characterisation

#### 5.2.7.1. Rheology measurement

The rheological properties of the ink used for the inkjet printing were tested using HAAKE MARS40 rheometer (Modular Advanced Rheometer System, Typ006-3098, Germany) coupled with a double gap cylinder rotor (CC27 DG/Ti) and a double gap cup (CCB27 DG/SS). The measurements were performed at 25 °C in duplicate according to a constructed

setup program. The program consisted of five consecutive steps: heating up to 25 °C (30 s), rotation at 10.00 s<sup>-1</sup> (50 s), linear rotation ramp from 0.1000 s<sup>-1</sup> to 1000 s<sup>-1</sup> (50 s), rotation at 1000 s<sup>-1</sup> (50 s), and a linear rotation ramp from 1000 s<sup>-1</sup> to 0.1000 s<sup>-1</sup> (50 s). The data was fitted according to the Herschel-Bulkley curve fit model.

#### 5.2.7.2. Surface tension

The surface tension of the ink solutions was measured at 24.2±0.7 °C in triplicate for each ink solution (PG20, PG40 and purified water). The pendant drop method was applied using the contact angle goniometer CAM 200 (KSV Instruments Ltd., Finland, currently known as Biolin Scientific). A 5 µl drop was dispensed from a disposable plastic tip (Fintip 200 µl, Thermo Scientific, Finland) and imaged for 10 s. The drop shape was recorded with a camera (AS021-2, Basler, Germany) and was fitted to the Young-Laplace equation using the OneAttention software (Theta1.4) to calculate the surface tension of the ink.

#### 5.2.7.3. Jettability of ink

After an initial characterization of the physical fluid properties was done an indication of printable PG and water combinations was gained by calculating the Z-value using *Equation 3* [54]. The Z-value relates the physical properties of the ink (density ρ, surface tension γ, viscosity η) and, the nozzle diameter (α) of the print head with the droplet formation.

$$Z = \frac{1}{oh} = \frac{Re}{\sqrt{We}} = \frac{\sqrt{\alpha\rho\gamma}}{\eta}, \quad (3)$$

$$Re = \frac{v\rho\alpha}{\eta},$$

$$We = \frac{v^2\rho\alpha}{\gamma},$$

The Z-value alone cannot be used to define the jettability as there are different combinations of densities, viscosities, and surface tensions that can have the same Z-values. The velocity of the ejected droplet needs to be taken into account when calculating the Z-value for the Reynolds (Re) and Weber (We) values for a more accurate prediction. However, the velocity (v) of the ejected droplet from the print head was not considered in the calculations for this study.

#### 5.2.7.4. Ink-substrate interactions

An initial test series of the contact angle measurements was conducted with purified water, PG20 and PG40 on SC, NF, SCBB and SCNF substrates. The test series included both non-crosslinked and UV-crosslinked, as well as thermally crosslinked samples, of all the

previously mentioned samples (n=1). The contact angle was measured at  $23.6\pm 1.0^\circ$  according to the sessile drop method using the same goniometer as mentioned for the surface tension.

After the initial testing series, additional measurements (n=3) were conducted with water and PG40 on thermally crosslinked substrates (SC, BB, NF SCBB, SCNF), as well as on non-crosslinked SC samples with water and PG40 (as reference), as these were most relevant for the final purpose. The reference was also used for checking any trendline changes in the contact angle between crosslinked and non-crosslinked samples.

### 5.3. Statistical analysis

A statistical two-tailed t-test assuming unequal variances was used to analyse the statistical significance ( $p > 0.05$ ) of the results wherever applicable. Microsoft Office Excel 365 ProPlus was used for the analysis.

## 6. Results and discussion

### 6.1. Physical properties of the substrates and their combinations

#### 6.1.1. Electrospun fibres

The NF substrates (*Figure 4*) were prepared from solution A using the eS-robot<sup>®</sup> electrospinning machine. The thermal crosslinking changed the appearance of the fibre substrate, as can be seen in *Figure 4A*. The most obvious visual change is the colour shifting from white to yellow upon thermally crosslinking the fibres (*Figure 4A*). This is due to changes in the arrangement of some easily macromolecular groups that can undergo chain scission because of the high heating temperature [52][55] and applies to all substrates (SC, BB and combinations). However, the SEM image taken of the fibres after crosslinking (*Figure 4C*) showed no visible changes in the fibre morphology. Mirafatab *et al.* [52] reported that nanofibres electrospun from only PVA became brittle and fragile to the touch after thermal crosslinking. This was not seen for the thermally crosslinked substrates in this study, due to the addition of SA to the mixture.

Nanofibres were also electrospun onto SC films. The SC film surface did not affect the electrospinning processes and the properties of the fibres. However, the electrospinning process required the SC film to be cast on aluminium foil instead of copier film so that the fibres would adhere to the surface.

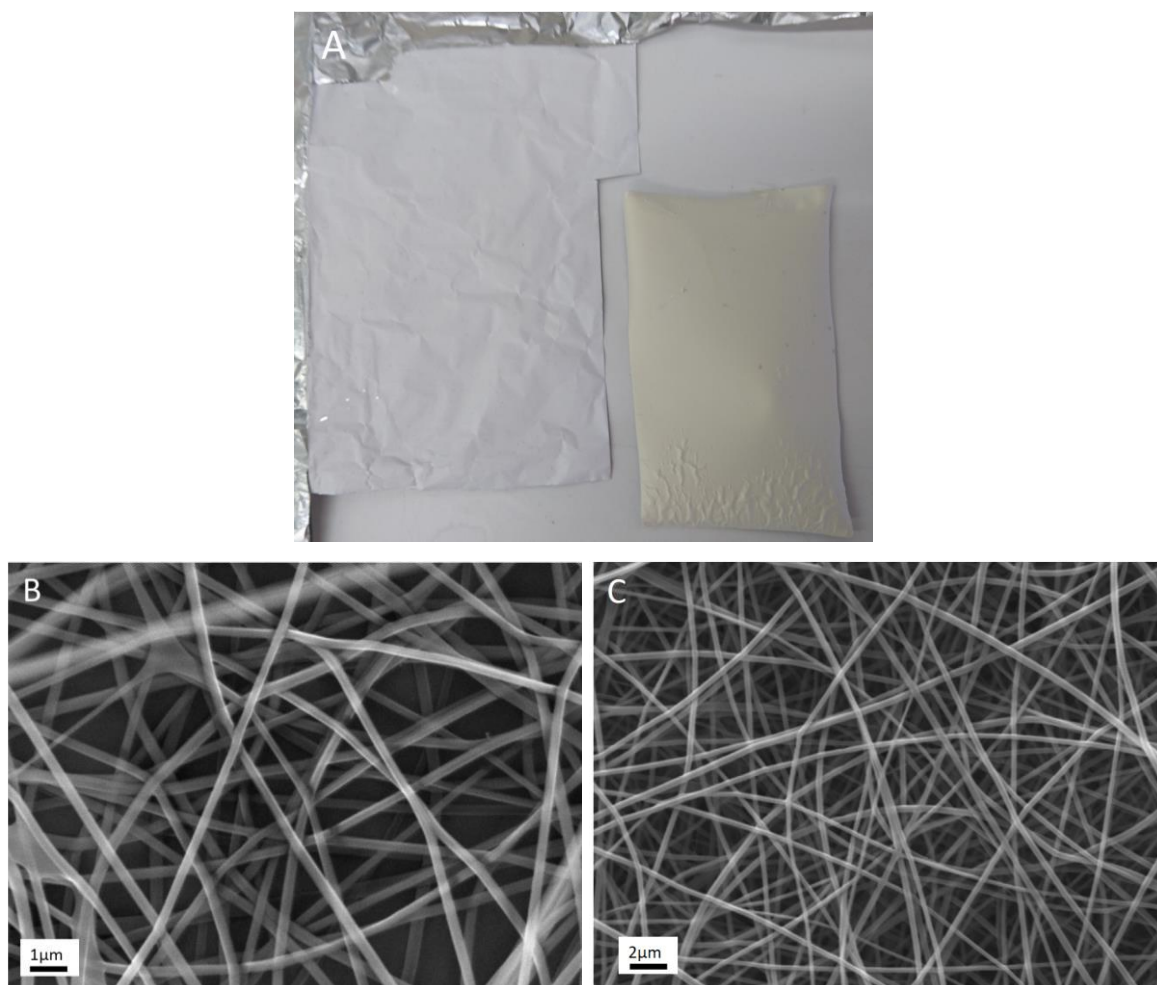


Figure 4. Nanofibre substrates on aluminium foil. A) Photographic image of non-crosslinked fibres (left) and thermally crosslinked fibres (right). B) Scanning electron microscopy (SEM) image of non-crosslinked nanofibres (20000 $\times$  magnification). C) SEM image of thermally crosslinked nanofibres (10000 $\times$  magnification).

The fibres appear separately except for a few merges that can be seen here and there (*Figure 4B, upper left quadrant*) as a result of the drying of the solution when collected onto the foil during electrospinning. The diameter of the non-crosslinked fibres was uniform in a range of  $267\pm 61$  nm (*Figure 5B*).

The average fibre diameter was  $311\pm 84.8$  nm for the crosslinked fibres (*Figure 5CD*). There was a slight difference in the average fibre diameter between the crosslinked and the non-crosslinked fibre substrates. However, it is needed to mention that the SEM images were taken with different equipment and coating methods, which may cause some differences that were not taken into account when measuring the fibre diameter. The difference could also be due to the variation in ambient conditions during the electrospinning.

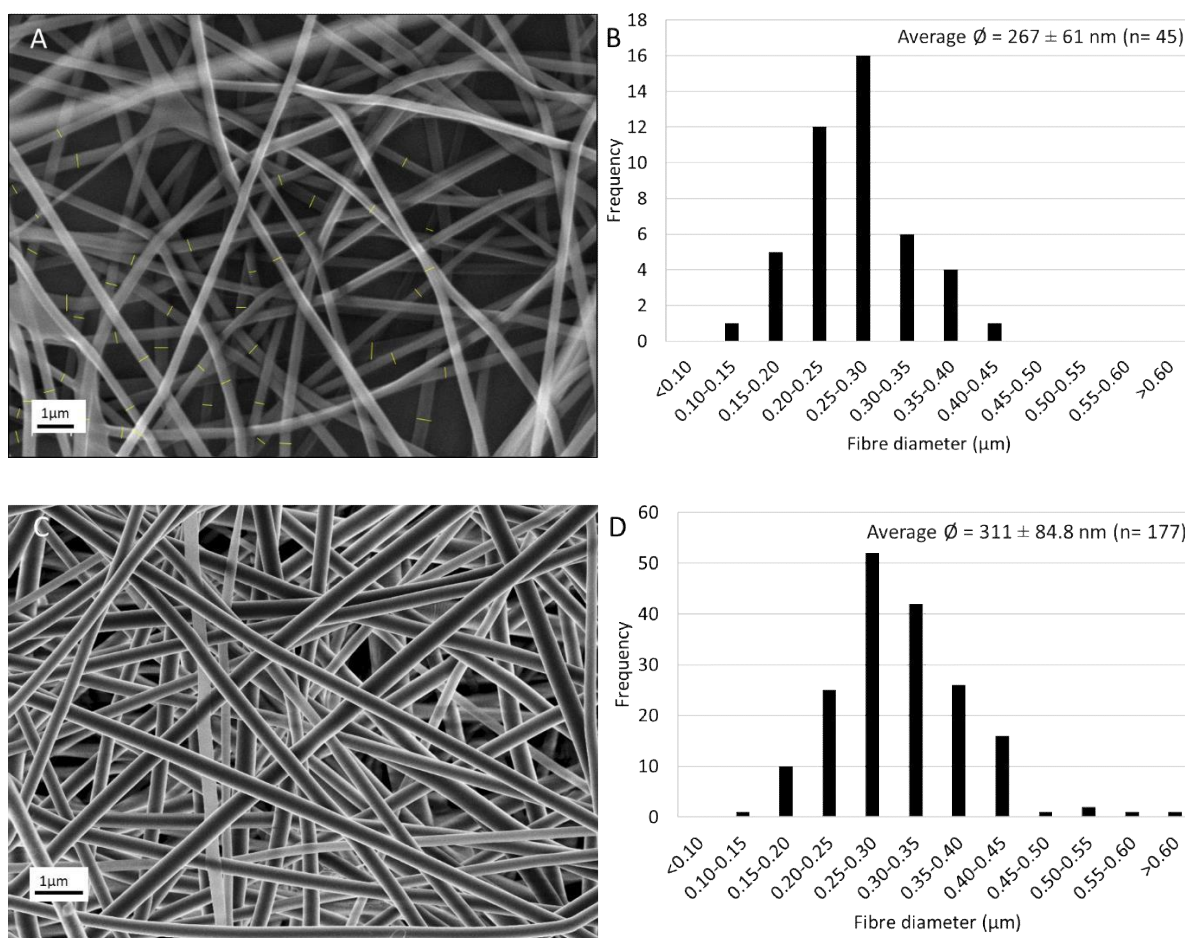


Figure 5. A) Scanning electron microscopy (SEM) image of non-crosslinked nanofibres (NF, 20000x magnification) and B) fibre diameter distribution of non-crosslinked NF. C) SEM image of crosslinked NF (10000x magnification), and D) fibre diameter distribution of crosslinked NF.

### 6.1.2. Solvent cast films

For selecting a suitable casting setup for the SC substrates, different solutions and wet heights were compared. Solution B was much thicker than solution A, which made the preparation process and mixing more difficult. The drying time varied according to the wet height and the viscosity of the solution. Films from solution B took longer to dry since the solution was more viscous, but the thickness also played a role as the films cast from solution A with a wet height of 1000 μm also dried more slowly. Air bubbles occurred during casting in some of the films cast from solution A. The amount of bubbles in the cast films increased with the viscosity of the solution, as bubbles appeared more frequently in films cast from solution B. The films made from solution B with the wet height of 500 μm were more difficult to cut into samples, because they started curving and did not stay flat. Therefore, films made from solution A were chosen. The dried and crosslinked films cast from solution A with a wet height of 500 μm are shown in *Figure 6*. The results from the puncture test also indicated that the films made from solution A with a wet height of 500 μm possessed

desirable mechanical properties for further use (*Table 1*). These were easy to handle, not too brittle but not too strong either for the desired purpose. The mechanical properties of the films were important as the films were used as a base layer for the bi-layered structures, adding the 3D printed structure and the nanofibres on top.

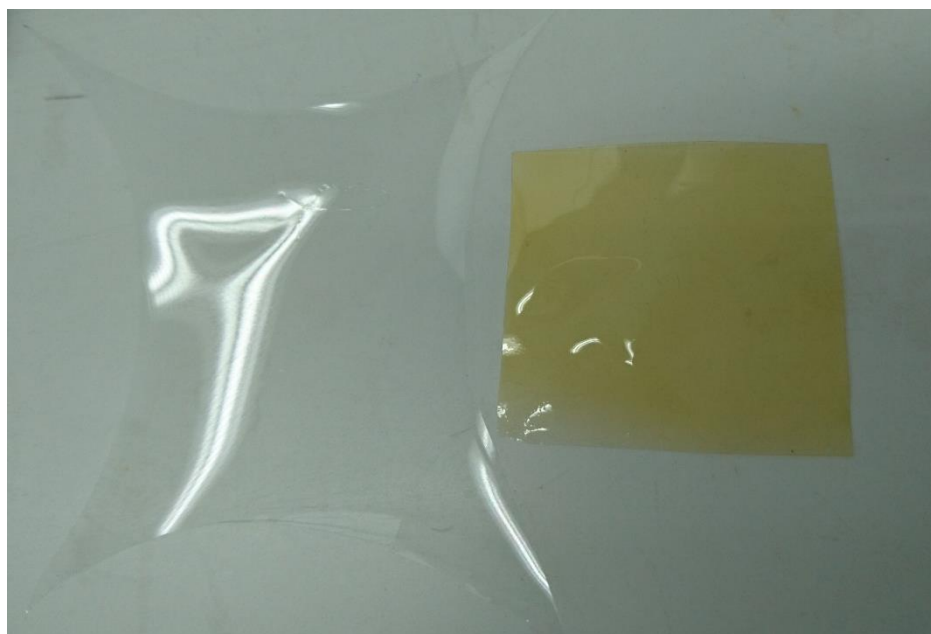


Figure 6. Photographic image of non-crosslinked (left) and crosslinked (right) solvent cast (SC) substrate.

Table 1. Thickness, break force and break distance of the solvent cast (SC) films prepared with different casting variables ( $n=20$ ).

Solution type	Wet height ( $\mu\text{m}$ )	Thickness (mm)	Break force (N)	Break distance (mm)
Solution A	500 $\mu\text{m}$	$0.53\pm 0.1$	$55.5\pm 23.7$	$6.88\pm 2.4$
	1000 $\mu\text{m}$	$0.78\pm 0.06$	$104.0\pm 14.4$	$10.1\pm 1.4$
Solution B	500 $\mu\text{m}$	$0.47\pm 0.05$	$50.2\pm 16.5$	$6.3\pm 2.3$
	1000 $\mu\text{m}$	$0.82\pm 0.13$	$108.6\pm 19.9$	$10.3\pm 2.7$

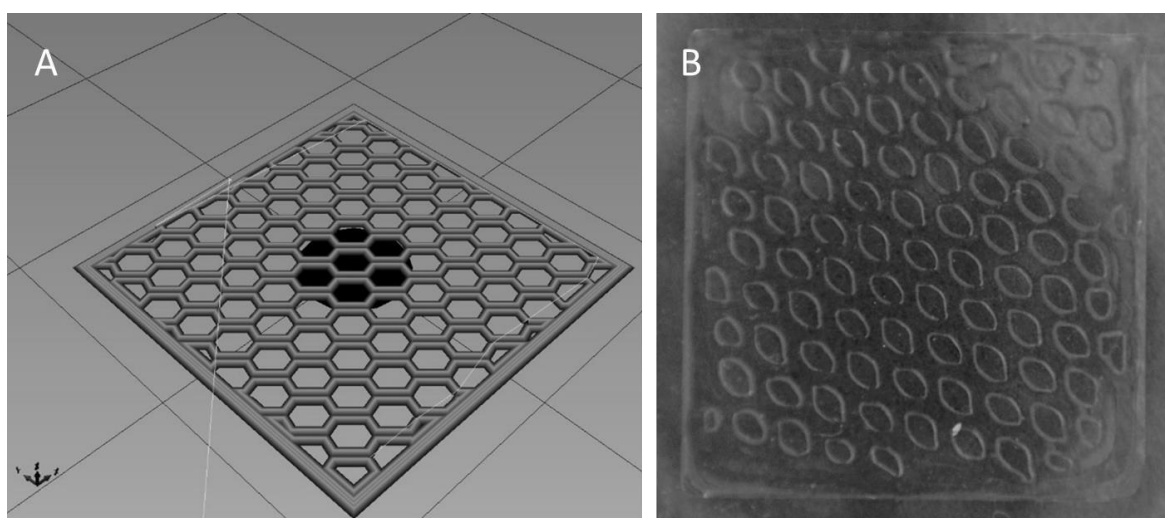
The SC substrates showed good thickness uniformity (*Table 1*). However, when analysing the relationships between the thickness of the substrates and the break force or the break distance, no apparent correlation could be seen. This indicates that there are other factors affecting the mechanical strength properties of the films, such as the drying process. The airflow, time, and relative humidity are important factors that affect the thickness and



mechanical strength of the films. The volatility of the solvent and the retained amount of solvent in the film also affect the mechanical properties of the films [56].

### 6.1.3. Three-dimensional printed substrates

For preparing the 3D printed (BB, SCBB) substrates, solution B was used due to the need of a higher viscosity to fit the semi-solid extrusion printer. The design of the  $1.65 \times 1.65$  cm single-layered square was prepared using FreeCAD<sup>®</sup> software. The square prototypes were sliced with a 40% honeycomb infill model to achieve a grid-like pattern to achieve a more porous structure (*Figure 7*). The BB substrates were printed on commercial copier films and, thus, creating a porous structure once dried and removed from the commercial copier film.



*Figure 7. A) Designed three-dimensional (3D) structure of the 3D printed (BB) substrates with a 40% honeycomb infill pattern. B) Microscopy image of the whole area of the non-crosslinked BB substrate.*

The non-printed area after drying was calculated from microscopy images using ImageJ to find out how much the structure deviated from the original design (*Figure 7*). The 40% infill pattern should have left 60% of the inner area of the design uncovered. This means that the theoretical non-printed area would constitute  $0.85 \text{ cm}^2$  out of the total area ( $2.7225 \text{ cm}^2$ ). The analysis of the microscopic images with ImageJ (freehand selection of area) showed that, in practice, the non-printed area constituted only approximately  $0.66 \text{ cm}^2$  ( $n=2$ ). This means that the printed structure did not completely retain its designed shape, and thus, reduced the size of the macropores structure somewhat. One explanation to this may lie in the viscosity not being high enough for the solution to stay in the printed shape. Another thing to keep in mind is that ejecting the solution out of the small needle tip affects the viscosity compared to the initial behaviour of the solution due to high shear forces applied.

The SCBB substrates were prepared by printing 3D structures on top of the SC films, creating a bi-layered structure. The two layers of the crosslinked SCBB substrate stuck nicely together and did not separate from each other. The printed layer on top of the film formed small cavities on the surface.

## 6.2. Puncture test

A puncture test was performed on non-crosslinked and crosslinked samples of SC, BB, SCBB and SCNF to investigate the mechanical properties of the substrates. The force needed to break the crosslinked SC samples was very similar to the break force of the non-crosslinked samples considering the substantial standard deviation of the samples (*Figure 8*). A statistical analysis confirmed that the difference between the crosslinked and non-crosslinked substrates was statistically not significant. This applied to all the different substrates when comparing the crosslinked substrates with the non-crosslinked ones. The thickness varied considerably for the SC samples, especially for the crosslinked substrates.

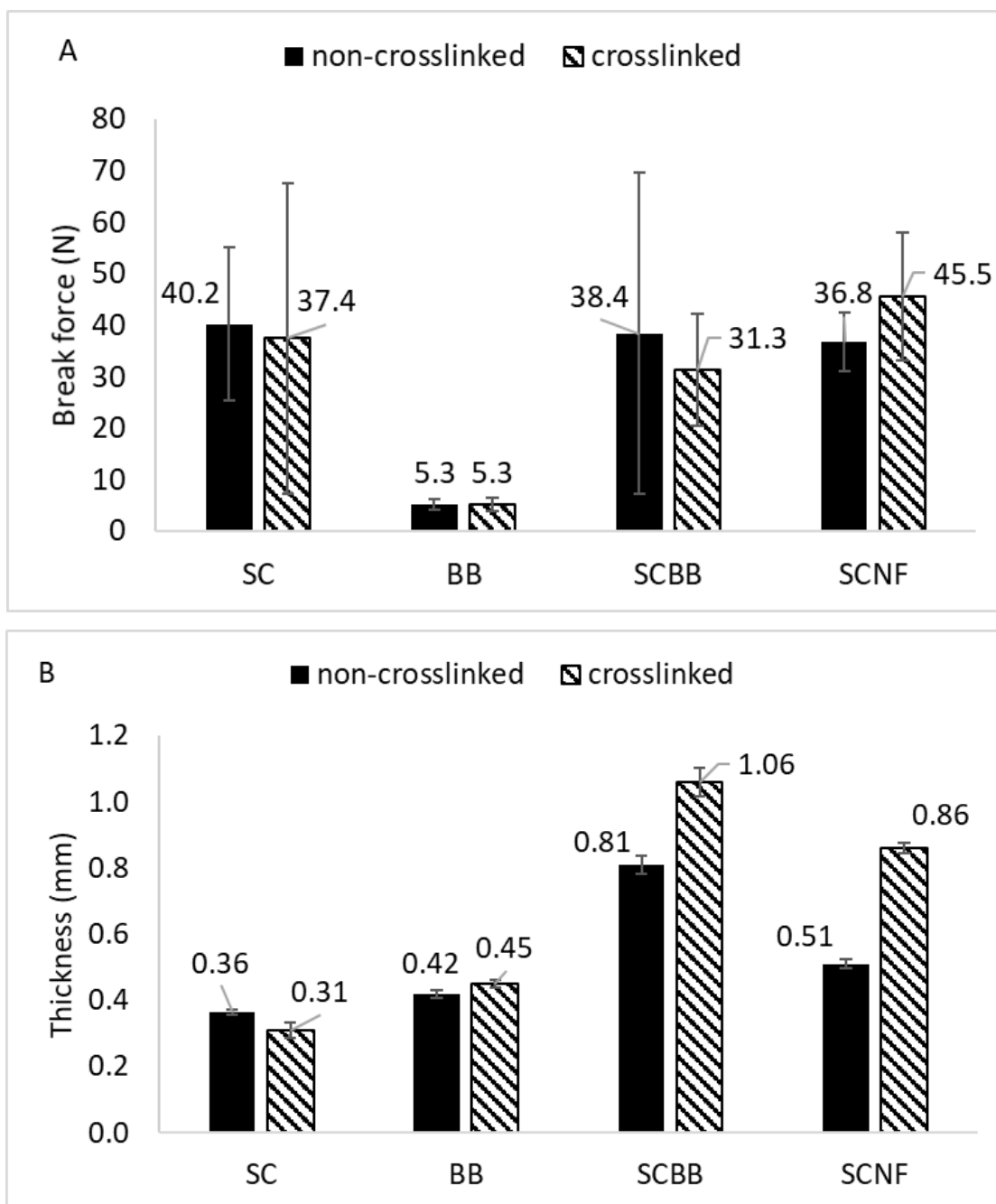


Figure 8. A) Average break force (N) for the non-crosslinked and crosslinked solvent cast (SC), 3D printed (BB), bi-layered solvent cast/3D printed (SCBB) and solvent cast/nanofibre substrates (SCNF) (n=10). B) Thickness (mm) of the SC, BB, SCBB and SCNF substrates (n=10).

The break force was equally small for both crosslinked and non-crosslinked BB substrates. Their thickness did not vary much, either. It can be noticed that their mechanical strength is low, which was expected because of the macroporous structure. The break force for the SCBB substrates had a high standard deviation for the non-crosslinked substrates, whereas the deviation was lower for the crosslinked ones. This could be most likely due to the differences in the SC films (factors mentioned previously in section 6.1.2) rather than with the effect of combining the two substrates. The break force of the BB substrates was almost

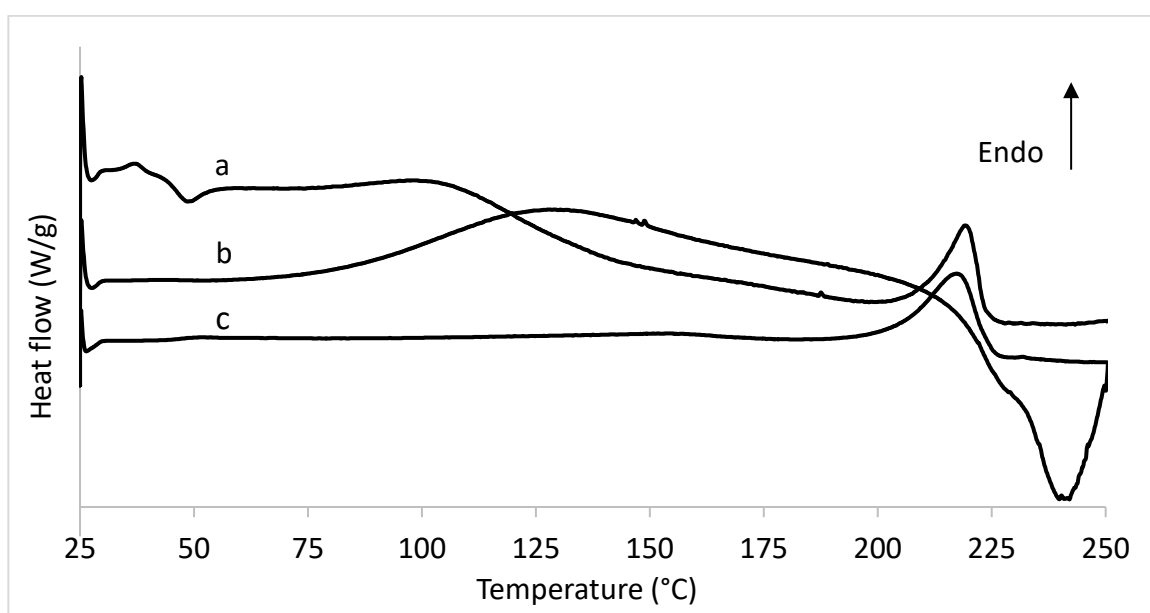
neglectable compared to that of all the other substrates; therefore, it hardly affected the break force of the SCBB substrates even though the uniformity (thickness, position and appearance of pores after drying) of the BB substrates varied due to the preparation method. In the bi-layered SCBB substrate, the addition of the 3D printed layer on top of the SC film did not give a statistically significant difference in the physical properties. The same applied to the bi-layered SCNF substrate, where adding the fibres to the SC film had no significant effect on the mechanical strength of the substrate. However, the thicknesses of the non-crosslinked SCNF and the crosslinked SCNF substrates showed a statistically significant difference ( $p=0.00004$ ). This indicates that bi-layered structure is affected by the thermal crosslinking. The changes are most likely related to the fibre layer as a similar variation was not seen in the thickness of the single SC substrates. Unfortunately, it was not possible to perform the puncture test for the separate fibre layer due to the difficulties of removing it from the aluminium foil. This measurement could have given some insight into the mechanical strength of the fibres alone.

### 6.3. Stability of the substrates

#### 6.3.1. Differential scanning calorimetry

The thermal analysis of the substrates was performed to study the changes in the thermal properties of the substrates over time. The long-range order between chains is characterized by crystallinity. In a crystallinity fusion, with rising temperature, a sharp change occurs from an ordered solid state to a more disordered liquid state. This transition is not so sharp for macromolecules, since polymers are usually not completely crystalline, but composed of crystalline and amorphous domains. The presence of crystallinity can be increased by thermomechanical processing, which allows for the chains to stack up in an optimal alignment. The glass transition temperature ( $T_g$ ) is apparent in the amorphous domains of polymers and is detected as a step on the baseline of the thermogram. This event corresponds to the transition from a disordered rigid solid to a more flexible one. The mobility change is however often a weak event for solids and requires the most sensitive apparatus found on the market. PVA is a semi-crystalline polymer where only the amorphous domains are concerned by glass transition. Therefore, the transition is weakened and broadened out. The  $T_g$  for PVA would have been seen around 87 °C, but as said much sensitive apparatus is needed for solids to reveal the  $T_g$ . In *Figure 9*, the endothermic melting phase transition ( $T_m$ ) of PVA was observed as a peak at 217 °C with an enthalpy change of  $\Delta H \approx 75$  J/g, which is

in accordance to previous results [57]. The heat required for melting of 100% crystalline PVA is 138.6 J/g, which means the nominal value of crystallinity obtained from the DSC thermogram was close to 54% [52][58]. SA is an amorphous material that decomposes in two separate steps. The dehydration of SA is seen as an endothermic peak around 100 °C [59] after which the decomposition of the biopolymer takes place. The decomposition is characterized by an exothermic peak around 240-260 °C. These peaks were seen in the DSC curves of SA at 120 °C and 242 °C, respectively (*Figure 9*). The decomposition leads to carbonaceous Na<sub>2</sub>CO<sub>3</sub> residue with a decomposition temperature above 750 °C under N<sub>2</sub>.

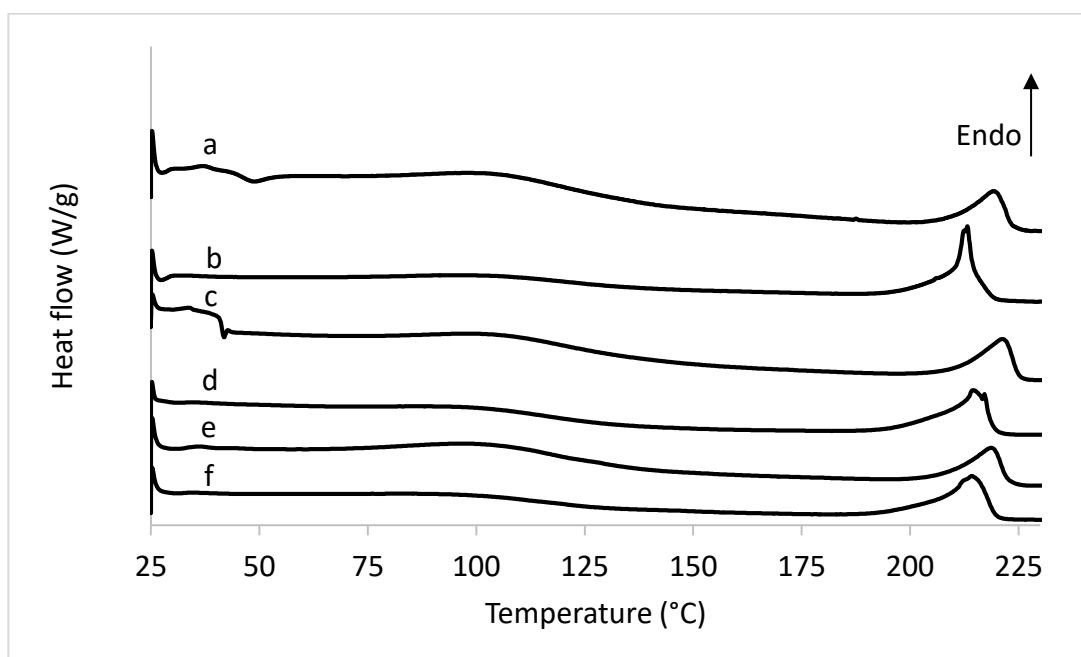


*Figure 9. Differential scanning calorimetry (DSC) thermograms of a) non-crosslinked electrospun nanofibrous (NF) substrate b) sodium alginate and c) polyvinyl alcohol. Thermograms are offset in heat flow for clarity.*

The dehydration step of the non-crosslinked NF substrate shifted from 120 °C to 99 °C. This probably covers whatever mobility change ( $T_g$ ) that could have been observed, as the fibres are mostly amorphous [60]. The  $T_m$  of the non-crosslinked NF substrate was observed at 219 °C and corresponded well to previous results [60]. Decomposition of the NF did not occur (at least within the measured temperature range) which indicates inter- and intramolecular hydrogen bonds between the polymers.

The DSC thermograms of the NF substrates from the stability study showed that thermal crosslinking stabilized the nanofibrous polymer structure in terms of thermal properties (*Figure 10*). Water molecules were incorporated into the fibrous structure during 1 month of storage in wet conditions (40 °C, RH of 75%), which was seen as an increase in the  $T_m$  to 221.3 °C for the non-crosslinked substrate (*Figure 11*). Whereas the  $T_m$  of the crosslinked NF substrate stored at the same conditions was 214.5 °C (*Figure 11*). The NF substrates

stored in dry conditions (RT, RH of 0%) showed the same trend. The  $T_m$  of the non-crosslinked and crosslinked NF substrate was 218.7 °C and 214.2 °C, respectively (*Figure 10*).



*Figure 10. Differential scanning calorimetry (DSC) thermograms of electrospun nanofibres (NF): a) non-crosslinked NF, b) crosslinked NF b) non-crosslinked NF stored for 1 month at 40 °C and relative humidity (RH) of 75%, c) crosslinked NF stored for 1 month at 40 °C and RH of 75%, d) non-crosslinked NF stored for 1 month at room temperature (RT) and RH of 0%, and e) crosslinked NF stored for 1 month at RT and RH of 0%. Thermograms are offset in heat flow for clarity.*

The DSC thermograms of the SC substrates from the stability study showed that the SC films are stable regardless of the storage conditions or crosslinking (*Figure 11*). The  $T_m$  of the SC substrates did not change over time in different storage conditions. The initial  $T_m$  for the non-crosslinked SC substrate was 217.3 °C (*Figure 11*) and the initial  $T_m$  for the crosslinked SC substrate was 213.2 °C, whereas the  $T_m$  for all the other substrates varied within 217.2-217.7 °C range. With this measurement setup, the  $T_g$  events were overlapping with the dehydration of the substrates. No clearly defined decomposition events of SA could be detected for these substrates either. However, some decomposition was detected at temperatures above the  $T_m$  for the non-crosslinked SC substrates stored at dry conditions and for the crosslinked SC substrates.

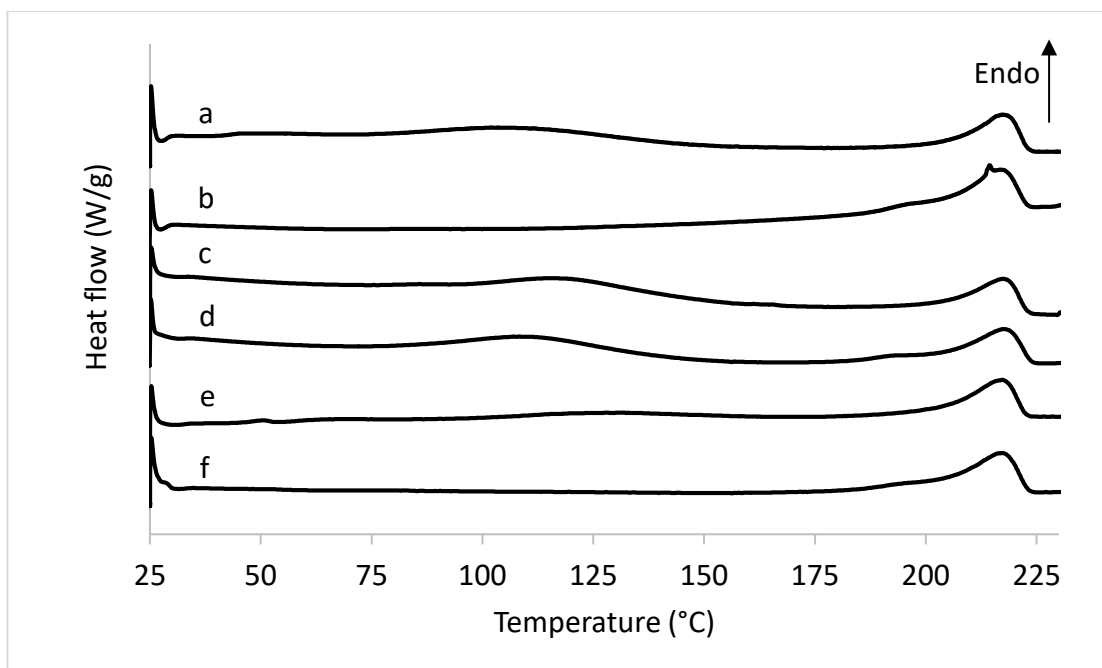


Figure 11. Solvent cast film substrates (SC) a) non-crosslinked SC, b) crosslinked SC c) non-crosslinked SC stored for 1 month at 40 °C and relative humidity (RH) of 75%, d) crosslinked SC stored for 1 month at 40 °C RH of 75%, e) non-crosslinked SC stored for 1 month at room temperature (RT) and RH of 0%, and f) crosslinked SC stored for 1 month at RT and RH of 0%. Thermograms are offset in heat flow for clarity.

### 6.3.2. Infrared spectroscopy

An in-depth IR analysis of the substrates included in the stability study was done to investigate structural changes in the solid state over one month. Several characteristic peaks were identified from the IR spectra of the raw materials and their PM (Figure 12). The spectrum of pure SA displayed two characteristic vibrational peaks at  $1598\text{ cm}^{-1}$  and  $1407\text{ cm}^{-1}$ , due to stretching of the carboxylate group asymmetrically and symmetrically [33][61]. Skeletal signs were seen as a strong peak at  $1027\text{ cm}^{-1}$ . The IR spectrum of PVA showed a broad peak in the  $3550\text{--}3200\text{ cm}^{-1}$  region, originating from the O-H group of inter- and intramolecular hydrogen bonds (including those of water). A small peak at  $1734\text{ cm}^{-1}$  corresponds to the high hydrolysis degree of PVA (99%) with very few acetate groups present in the polymer chains [62]. The peak at  $1141\text{ cm}^{-1}$  has been proved to be related to the crystallinity of the structure [52][58][62]. The crystallinity degree offers a way of estimating the stability of the substrates over time and affect their stability in aqueous environment, i.e. at elevated humidity. Therefore, this is one of the most important characteristics to point out in the analysis of the stability of the substrates. The PM showed characteristic features of both SA and PVA. Peak broadening and intensity decrease of the band in the  $3500\text{--}3200\text{ cm}^{-1}$  region was observed. The asymmetrical stretch of C-O-C groups of SA at  $1027\text{ cm}^{-1}$  and  $1086\text{ cm}^{-1}$  were observed as a two-shouldered

peak in the spectrum of the PM roughly proportional in intensity to the blending ratio of the raw materials.

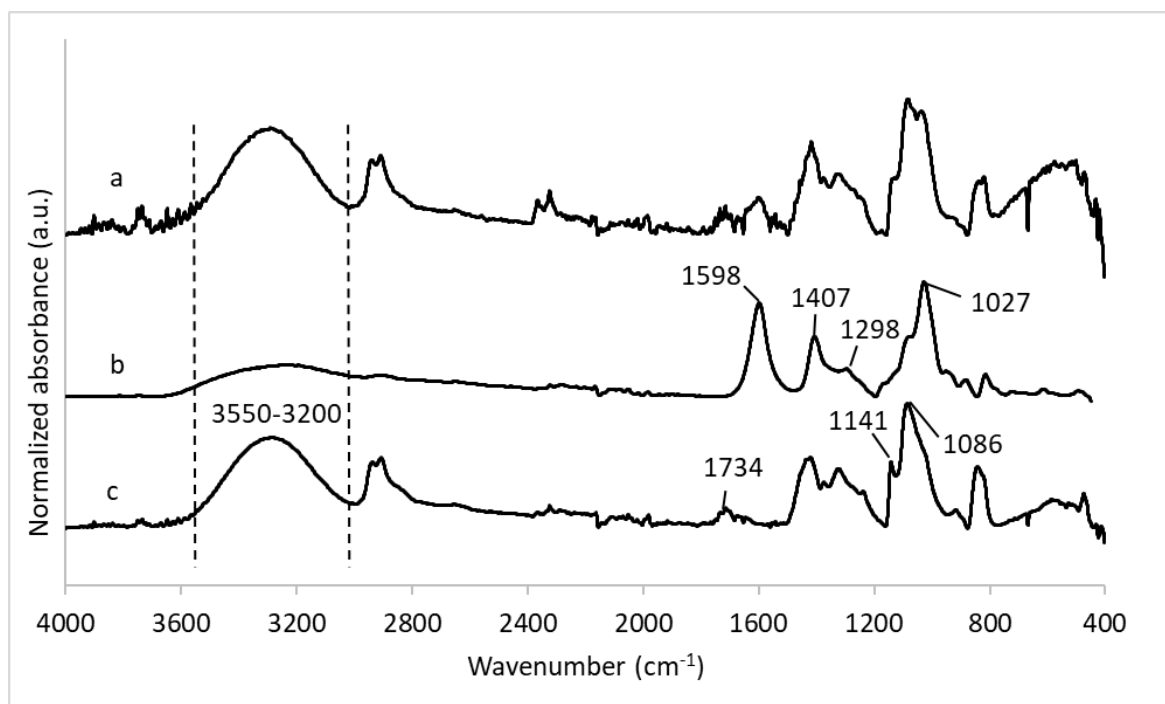


Figure 12. Infrared spectra of a) physical mixture of polyvinyl alcohol (PVA) and sodium alginate (SA), b) pure SA, and c) pure PVA. Spectra are offset in absorbance for clarity.

IR spectroscopy of the non-crosslinked and crosslinked NF substrates was performed to detect any peak shifts that could be connected to the interactions between the two blended polymers, including hydrogen bonding and/or any structural formations. The IR spectra of the non-crosslinked NF exhibited similar spectral features to those of the individual polymers, but some absorbance bands had shifted from their original positions in a similar way as in the spectrum of the PM (Figure 13). The non-crosslinked NF substrate was found to be amorphous, but the crosslinked NF substrate exhibited the characteristic peak connected to the crystallinity of the structure. The non-crosslinked SC substrates were found to be mostly amorphous exhibiting a small degree of crystallinity that increased after crosslinking. In Figure 13, this was seen from the presence of the crystallinity peak at  $1143\text{ cm}^{-1}$ .



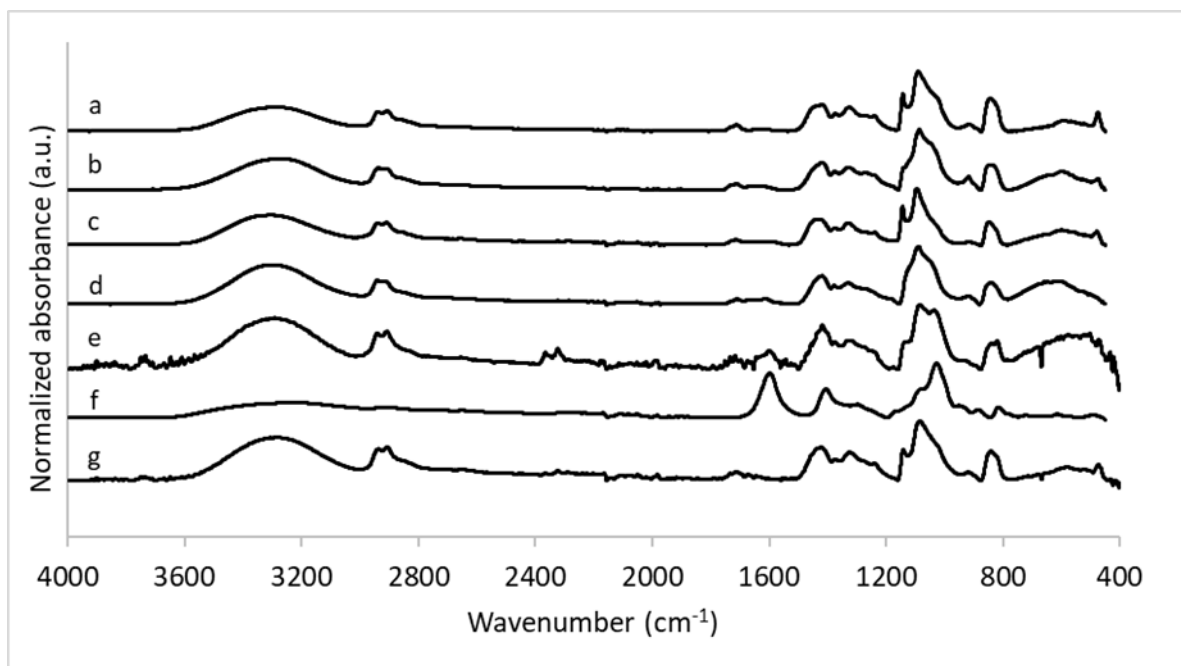


Figure 13. Infrared spectra of a) crosslinked solvent cast (SC) substrate, b) non-crosslinked SC substrate, c) crosslinked nanofibre (NF) substrate, d) non-crosslinked NF substrate, e) physical mixture of polyvinyl alcohol (PVA) and sodium alginate (SA), f) pure SA, and g) pure PVA. The spectra are offset in absorbance for clarity.

The stability of the substrates was studied by comparing the spectra taken from the substrates at different timepoints. The analysis showed that the initial NF substrate as well as the NF substrate stored in dry conditions were amorphous (Figure 14). Mirafteb *et al.* [52] found that the crystallinity of the fibres increased with higher crosslinking temperatures and heating time. Furthermore, it was concluded that physical crosslinking increases crystallinity categorically. This was seen for all the crosslinked NF substrates regardless of the storing conditions and time. Interestingly, a solid-state change from amorphous to crystalline was seen for the non-crosslinked substrates stored in wet conditions already after 24 h and the crystallinity increased over time for 1 month. This suggests that water and/or elevated temperature catalyse the crystallization of the substrates. The broad peak in the hydrogen bond region had a lower intensity than pure PVA, which probably correlates to the crosslinking and presence of SA. It could also be assigned to the lower water content in the substrate due to the heat treatment.

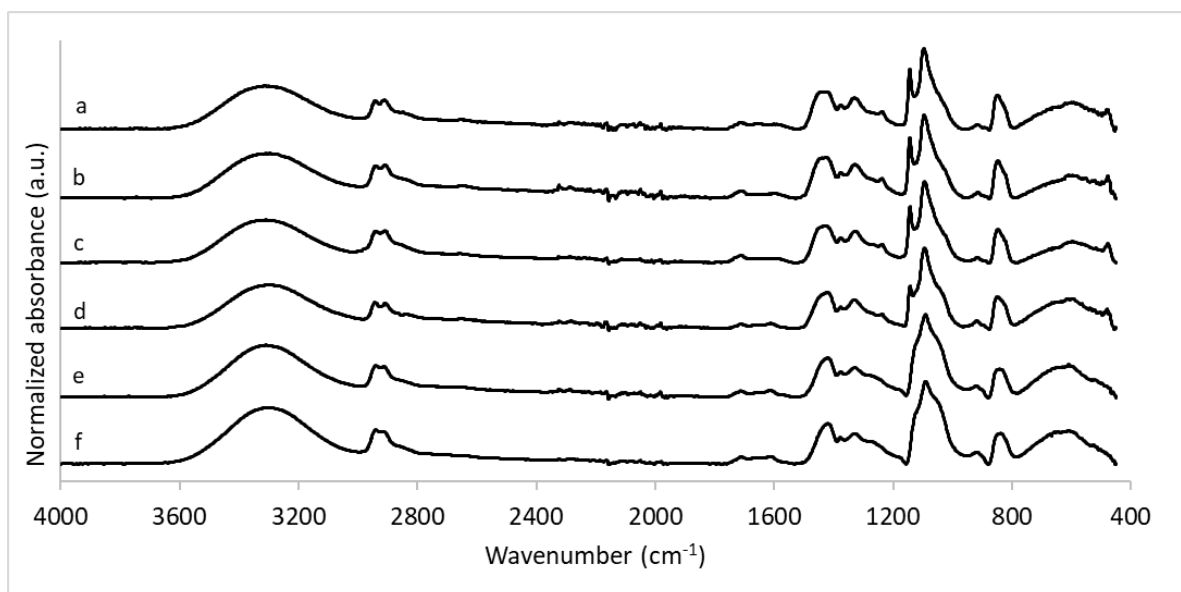


Figure 14. Infrared spectrum of a) crosslinked nanofibre (NF) substrate stored at wet conditions (40 °C, relative humidity (RH) of 75%), b) crosslinked NF substrate stored at dry conditions (room temperature, RH of 0%), c) crosslinked initial NF substrate, d) non-crosslinked NF substrate stored at wet conditions, e) non-crosslinked NF substrate stored at dry conditions, and f) non-crosslinked initial NF substrate. All samples were stored at said conditions for 1 month. Spectra are offset in absorbance for clarity.

The SC substrate yielded a spectrum where a few significant shifts were observed (Figure 15). There was a downwards shift of the carboxyl group in non-crosslinked and crosslinked SC substrates from  $1734\text{ cm}^{-1}$  to  $1619$  and  $1620\text{ cm}^{-1}$ , respectively. This correlates to the increased hydrolysis degree that occurs when the polymer is dissolved in water prior to solvent casting [62]. The crystallinity degree of the non-crosslinked SC substrates increased somewhat over time when stored in both dry and wet conditions (Figure 15B). Crosslinking made the SC substrates more crystalline and a clear peak was seen at  $1143\text{ cm}^{-1}$  for crosslinked SC substrates stored in both dry and wet conditions.

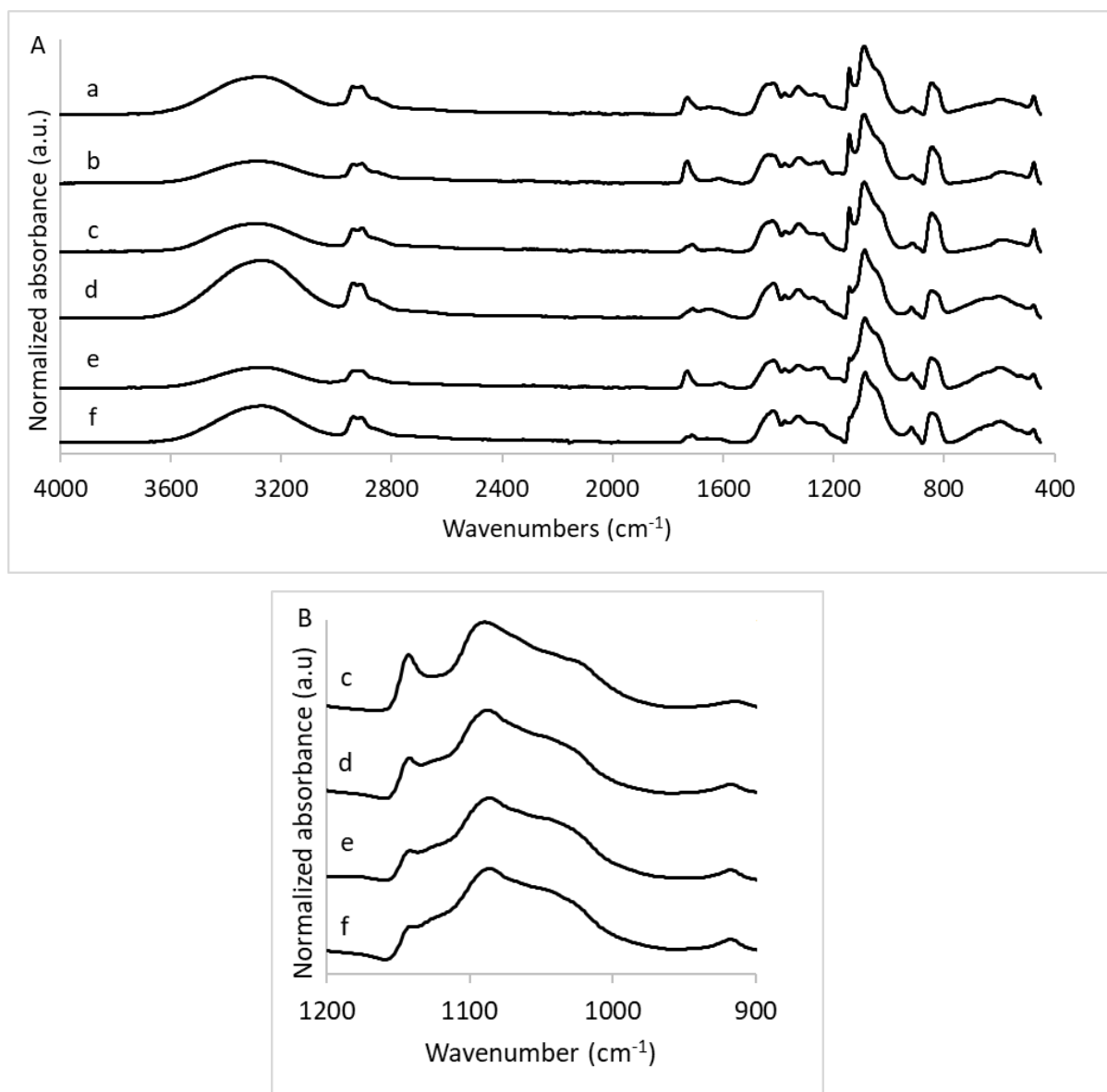


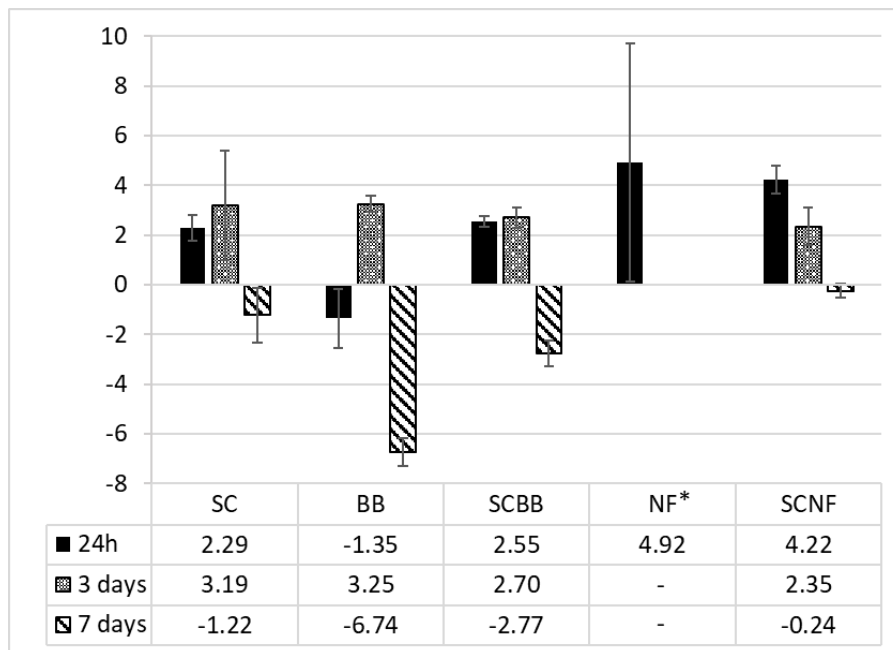
Figure 15. Infrared spectra in the spectral range of A) 4000-400  $\text{cm}^{-1}$  and B) 1200-900  $\text{cm}^{-1}$  of a) crosslinked solvent cast (SC) substrate stored at wet conditions (40 °C, relative humidity (RH) of 75%), b) crosslinked SC substrate stored at dry conditions (room temperature, RH of 0%), c) crosslinked initial SC substrate d) non-crosslinked SC substrate stored at wet conditions, e) non-crosslinked SC substrate stored at dry conditions, and f) non-crosslinked initial SC substrate. All substrates were stored for 1 month in said conditions. Spectra are offset in absorbance for clarity.

#### 6.4. Swelling and degradation of the substrates

The stability of the substrates in aqueous environment was tested by performing a swelling and degradation study. The non-crosslinked substrates did not maintain their structure after immersion into the PBS solution. The non-crosslinked BB sample disintegrated completely, whereas the other samples (SC, SCBB, SCNF) left small residual pieces in the solution after 24 h. However, the remains were not measured since it was not possible to collect the residue with the setup used. The thermally crosslinked samples remained intact (to the naked eye)

and were collected for weighing and further calculations on the swelling ratio and weight loss.

The samples of the SC substrate gained weight after 24 h (*Figure 16*). The weight continued to increase after 3 days of immersion in the media. After 7 days, the SC samples started to lose their weight probably due to the degradation of the film. Combining these results with the swelling ratio values for SC (*Figure 17*), there was an initial uptake of water (and/or salts from the buffer) after 24 h. However, this uptake decreased after 3 days and 7 days. This was probably due to the degradation process that started overtaking the swelling.



*Figure 16. Average weight loss (%) of the prepared substrates after 24 h, 3 days and 7 days (n=3). Negative value represents weight loss and positive value weight gain. Key: SC=solvent cast substrates, BB=3D printed substrates, SCBB=solvent cast/3D printed substrates, SCNF=solvent cast/nanofibres, NF=nanofibres. \*weighed with a different analytical balance.*

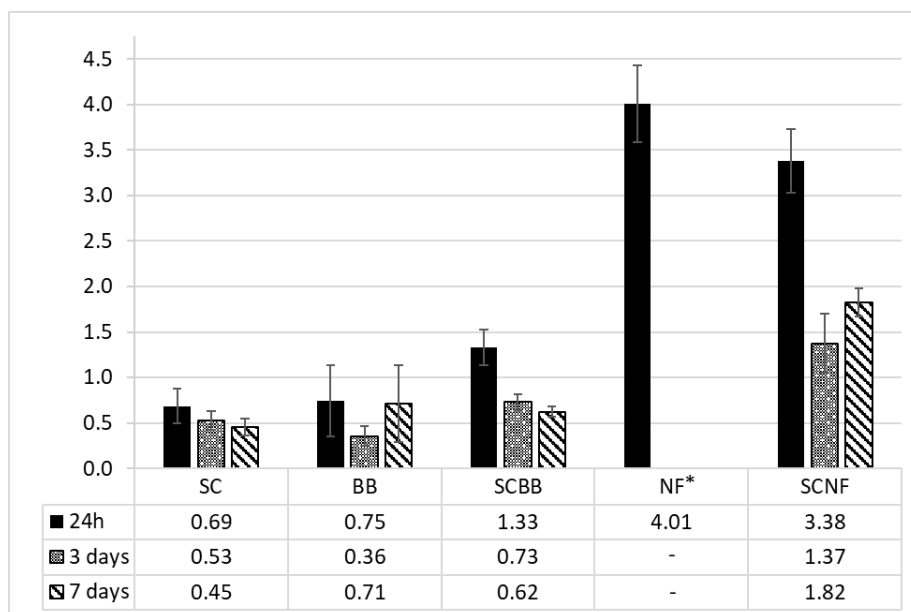
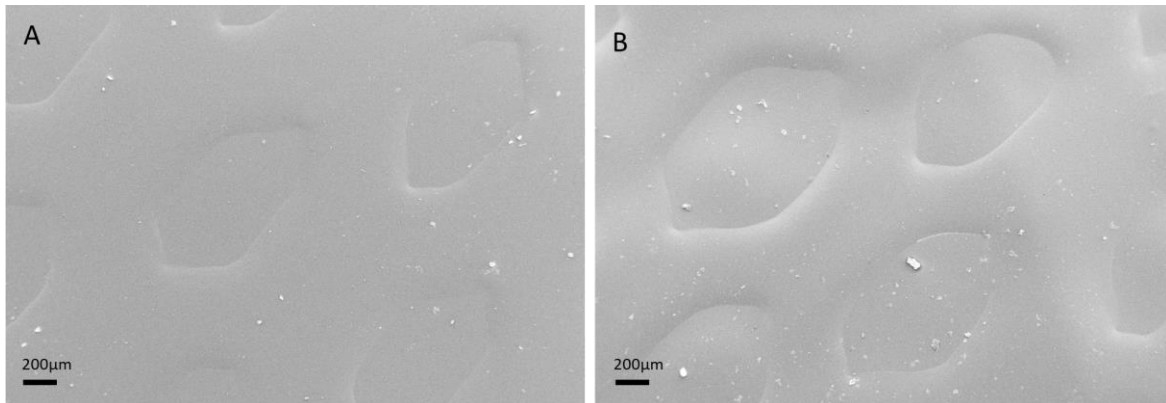


Figure 17. Average swelling ratio (g/g) of the prepared substrates after 24 h, 3 days and 7 days (n=3). Key: SC=solvent cast substrates, BB=3D printed substrates, SCBB=solvent cast/3D printed substrates, SCNF=solvent cast/nanofibres, NF=nanofibres. \*weighed with a different analytical balance

The BB substrates seemed to break down immediately after the first 24 h, and they were decreasing in weight. After 3 days, the weight increased again, possibly showing that the samples were taking up water and swelling. Although this did not correlate well with the swelling ratio, as the ratio was at the lowest ( $0.4 \pm 0.1$ ) after 3 days compared to the values obtained after 24 h ( $0.8 \pm 0.4$ ) and 7 days ( $0.7 \pm 0.4$ ) for the BB substrates. After 7 days the BB samples had lost approximately 7% of their initial weight indicating that they had started degrading. However, it should be noted that the standard deviation was quite high for the samples after 7 days of immersion. Due to the macroporous structure, the PBS solution had a larger contact with the substrates and it could be taken up faster compared to the other substrates.

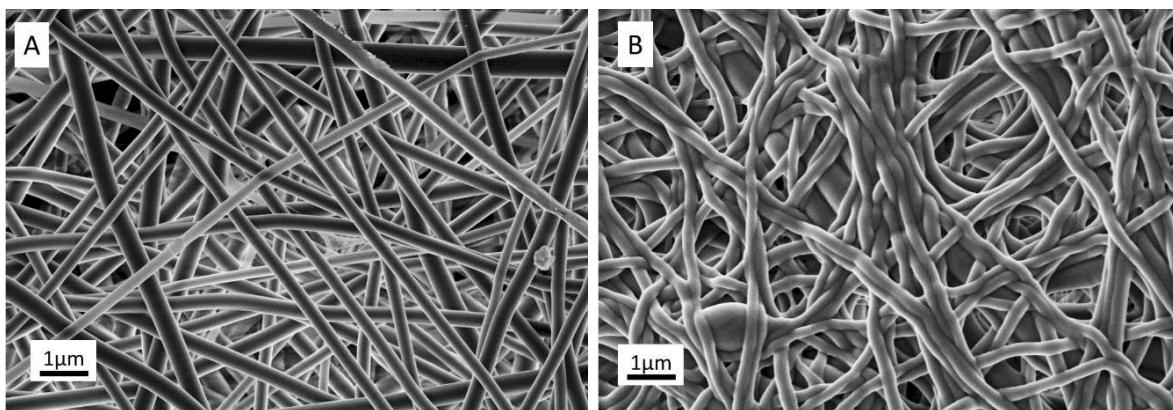
The weight of the SCBB samples increases by  $2.6 \pm 0.2\%$  after 24 h and stayed around the same level also after 3 days ( $2.7 \pm 0.4\%$ ). After 7 days, the samples started to lose weight and ended up  $2.8 \pm 0.5\%$  below their initial weight. After 24 h, the swelling ratio of SCBB showed high initial uptake of the solution probably because of the larger exposed surface area of the BB layer. The swelling ratio of the SCBB substrate stayed high after 3 days but then dropped down to  $0.6 \pm 0.1$  after 7 days. Presumably, the SC film minimized the contact between the PBS and the macroporous structure of the SCBB substrates compared to the BB substrates. Since the BB substrate is printed on top of the SC film, the macropores are closed off by the SC layer and therefore merely cavities are formed on the surface. This had an effect on the

degradation of the BB layer or both layers. The SEM images of SCBB substrates show that the two layers stuck together also after 7 days of degradation in PBS (*Figure 18*).



*Figure 18. Scanning electron microscopy images of A) the initial crosslinked solvent cast/3D printed (SCBB) substrate and B) dried SCBB substrate after 7 days in phosphate-buffered saline solution at 37 °C (30× magnification).*

The swelling of the NF substrates was studied only for 24 h, showing the largest swelling ratio of  $4.0 \pm 0.4$  out of all substrates. The substrates showed correlating weight gain of almost 5% after 24 h. The SCNF samples increased in weight (4.2%) the second most out of all the samples after the first 24 h (second to only NF). This correlated well to the high swelling ratio value of  $3.4 \pm 0.4$ , which was more than three times the initial weight. After 3 days, the weight started to decline and after the full week, the weight was 0.2% less than the initial weight. The swelling ratio followed the same declining trend and showed a value of  $1.8 \pm 0.2$  after 7 days, indicating degradation. After 7 days, the statistical analysis indicated no significant deviation from the initial weight of any of the substrates. The SCNF substrates consisted of individually detectable fibres after crosslinking (*Figure 19A*). The surface of the SCNF substrates after the degradation was smoother due to the swelling and adhesion of the NF (*Figure 19B*). No changes in the SC film were seen since the fibrous layer covered it.



*Figure 19. Scanning electron microscopy images of A) the initial crosslinked solvent cast/nanofibre (SCNF) substrate and B) dried SCBB substrate after 7 days in phosphate-buffered saline solution at 37 °C (10000× magnification).*

## 6.5. Adhesion of the substrates

In addition to good mechanical properties a substrate suitable for a wound dressing application, it must have the proper amount of adhesion skin. Ideally, the substrate should be self-adhesive (no need for coating), easy and painless to remove [53]. Crosslinking can enhance the adhesive force of polymers but may cause the material to harden and lose its ability to bond surfaces well [63]. An adhesion test was carried out to investigate the bioadhesion of the non-crosslinked and crosslinked substrates. The hydrophobicity of the substrate, level of hydration and rate of polymer erosion have been reported as the factors affecting the bioadhesion [3].

The max force required to detach the substrates from the artificial skin surface (detachment force) and the area under the force-time curve (work of adhesion) was calculated with the texture analyser program. The work of adhesion correlated directly to the detachment force and the results were applied as a measure of the bioadhesive performance of the substrates. The weakest detachment force was seen for the NF and SCNF fibre substrates (*Figure 20*). Low adhesion of the crosslinked substrates was seen because of the high polymer chain entanglement as the fibres started swelling when they came in contact with the artificial wound solution and thus reducing the availability of function groups of polymers to substrate [64]. The non-crosslinked SCNF exhibited similar detachment forces as the non-crosslinked SC substrates. This was probably due to dissolution of the non-crosslinked fibres on the SCNF. The non-crosslinked SC substrates proved to be most adhesive out of all, but crosslinking reduced the adhesion. This seemed to categorically be the case except for the BB substrates, where the crosslinked substrates were proved to be more adhesive than the non-crosslinked substrates. Since the non-crosslinked BB substrates did not retain their structure in an aqueous environment, as the results from the stability study showed, the increased adhesion values for the crosslinked BB substrates was probably seen as a consequence of them remaining intact upon contact with the artificial wound fluid as opposed to the dissolving non-crosslinked ones. The detachment force for all substrates was lower than that of the reference adhesives (*Figure 20*). A statistical significant difference in detachment force was seen for the BB, NF and SCNF substrates.

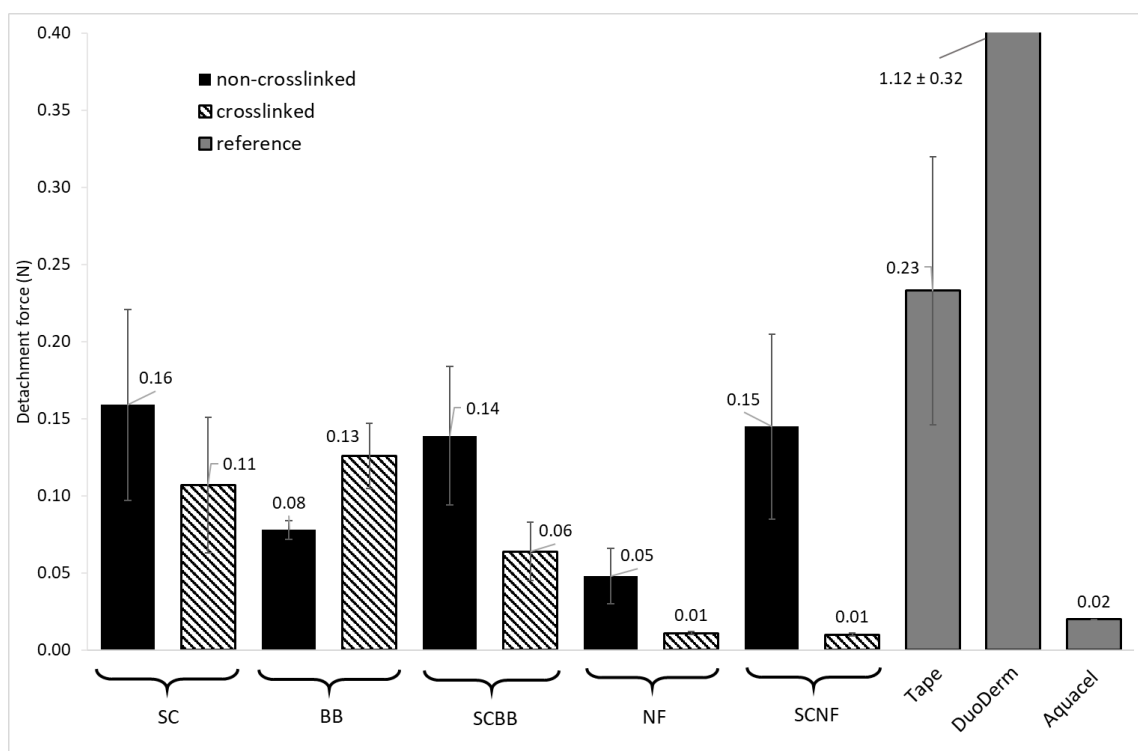


Figure 20. Adhesiveness as detachment force (N) of the non-crosslinked and crosslinked substrates, and DuoDerm™, Aquacel™ and double-sided tape (Scotch™) as commercial reference products (n=6). Key: SC=solvent cast film, BB=3D printed substrates, SCBB= solvent cast/3D printed substrates, NF=electrospun nanofibres, SCNF=solvent cast/nanofibre substrates.

## 6.6. Inkjet printing on the substrates

### 6.6.1. Ink properties

The properties of mixtures of water and PG were studied to evaluate their applicability for inkjet printing. The concentration of PG was found to have a linear correlation with the physiochemical properties of the ink base solutions (Table 2). An ink base solution of 40:60 (v/v) mixture of PG and purified water had been used for printing before and was therefore a natural choice [65]. The suggestions from the printer head manufacturer served as a reference for the viscosity [66]. The overall printability of the ink was predicted with the help of the calculated average z-value for the ink base solutions, taking the viscosity, surface tension and density of the ink solutions into account.

The PG40 expressed the most suitable properties for inkjet printing and has been used for printing before [65]. Here, the printing process was carried out with a stable jetting of the PG40 without any evident clogging. However, the surface tension affected the droplet ejection causing formation of satellite droplet tails from some of the printer nozzles. Based on previous research, ink suspensions with Z-values between 4 and 14 have reported to be printable [67].



Table 2. Physiochemical properties and the calculated Z-value (nozzle Ø 50 µm) for the ink base solutions with different concentration of propylene glycol (PG) added to water (MQ).

	Viscosity* (mPa·S)	Surface tension** (mN/m)	Average Z-value
MQ	1.0±0.1	73.8±0.3	61.2
PG10	1.5±0.1	61.0±0.4	37.3
PG20	1.9±0.1	55.9±0.3	27.6
PG30	2.8±0.1	51.0±0.4	18.3
PG40	3.9±0.1	47.4±0.1	12.6
PG50	5.6±0.1	45.1±0.0	8.6
PG60	9.5±0.0	42.0±0.4	5.0
PG70	11.1±0.1	40.8±0.5	4.2
PG80	13.3±0.1	39.6±0.3	3.5
PG90	16.2±0.1	38.5±0.0	2.8
PG	45.4±0.5	36.8±0.3	1.0

\*mean ± standard deviation, n=2, \*\* mean ± standard deviation, n=3

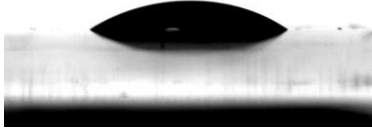
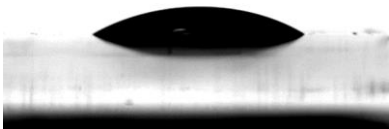


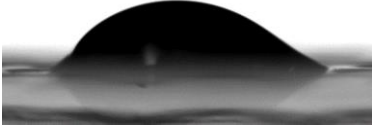
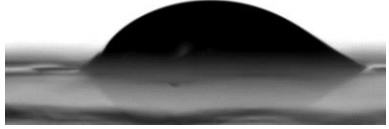



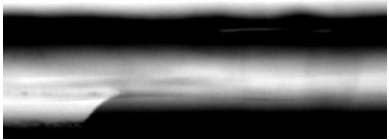
### 6.6.2. Contact angle

The initial series of single measurements with water, PG20 and PG40 was conducted to determine which substrates to include in the further measurements. The non-crosslinked NF substrates dissolved after the droplet was deployed on the surface, hence the contact angle could not be measured for the fibres themselves, as the droplet was resting on top of the aluminium foil underneath the fibres instead. The crosslinked NF and SCNF substrates absorbed both the water and the solutions with PG to a high extent and thus the contact angle could not be determined for these samples either. However, these samples were included in the second series of measurements, to confirm the results from the initial study. The UV-crosslinked samples were excluded from further measurements due to low crosslinking degree.

Contact angle measurements are best performed on flat surfaces; hence the results from the contact angle measurements for the SC substrates were very consistent (Table 3). As the BB and SCBB substrates were grid-shaped with cavities on the surface, the contact angle

measurement became dependent on location where the droplet landed on the surface. This was shown by the large standard deviation for the BB and SCBB substrates as well as the irregular shape of the droplets (*Table 3, "CL BB"*). The NF substrates absorbed most of the droplet within one minute as was seen in the initial measurements. Similar results were obtained for the non-crosslinked SCNF substrates. A thin and spread out droplet for both water and PG40 was detected on the surface after 5 seconds that completely absorbed after 60 seconds.

*Table 3. The contact angle of water (MQ) and ink base solution of 40% propylene glycol and water (PG40) on non-crosslinked (Non-CL) solvent cast (SC) film and crosslinked (CL) SC, 3D printed (BB) and solvent cast/3D printed (SCBB) substrates.*

	MQ* (°)	PG40*(°) 5 s	PG40*(°) 60 s
Non-CL SC	70.8±2.5	 35.9±2.5	 31.5±1.1
CL SC	58.3±1.1	 20.09±2.0	 17.4±0.6
CL BB	64.8±13.9	 30.7±11.3	 36.2±2.2
CL SCBB	48.5±3.8	 24.2±3.6	 20.9±2.8
CL SCNF	-	 -	 -

\* mean ± standard deviation, n=3

The addition of PG into the ink solution lowered the contact angle compared to the contact angle of water. In addition, the crosslinking also lowered the contact angle on the SC

substrates. The contact angle affects the spreading of the ink, which in this case refers to the fact that the addition of PG increased the spreading of the solution on the surface of the substrates. However, the crosslinking of the substrates makes the ink absorb less and therefore spread more on the intact polymer structure. The precision of the printing pattern is directly correlated to the contact angle and the spreading of the ink solutions. Thus, the interactions between the ink and the substrate need to be balanced for obtaining structures with a defined printed area.

### 6.6.3. Inkjet printing trial

It was observed that the coloured ink was well printable on the non-crosslinked SCBB substrates, probably dissolving the top layer of the substrate surface to a small extent. This was confirmed by the SEM images taken of the non-crosslinked and crosslinked SCBB substrates (*Figures 21,22*). The liquid evaporated step by step from the crosslinked substrates since the surface material did not absorb it and thus left behind a characteristic pattern of multiple circles much like the growth rings of a tree trunk. The droplets were also more circularly shaped on the non-crosslinked surface than on the crosslinked surface. The individual droplets (printed with 450 dpi) on the crosslinked SCBB substrate did not cover the printed area uniformly because the droplets merged together (*Figure 22*). Printing with the lower resolution of 100 dpi gave a better pattern than 450 dpi resolution printing. However, some of the droplets still merged together and the edges of the individual droplets were not sharply defined (*Figure 22*). The printing with 100 dpi resolution on top of non-crosslinked SCBB resulted in squares with sharp edges and extinguishable separate droplets (*Figure 21*). The droplets printed with 450 dpi resolution did not exhibit the same clarity in the position of the droplets.

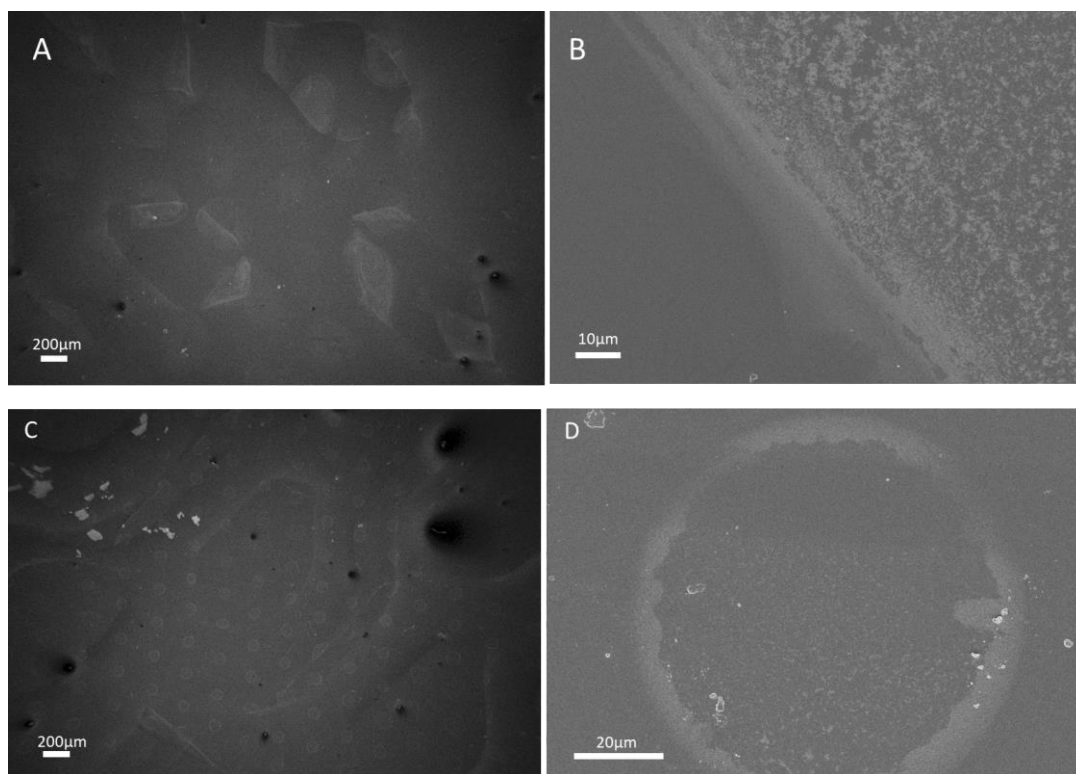


Figure 21. Scanning electron microscopy (SEM) images of inkjet printed samples with coloured ink on non-crosslinked solvent cast films/ 3D printed (SCBB) substrates printed with A-B) 450 dpi resolution and C-D) 100 dpi resolution (30× and 1000× magnification).

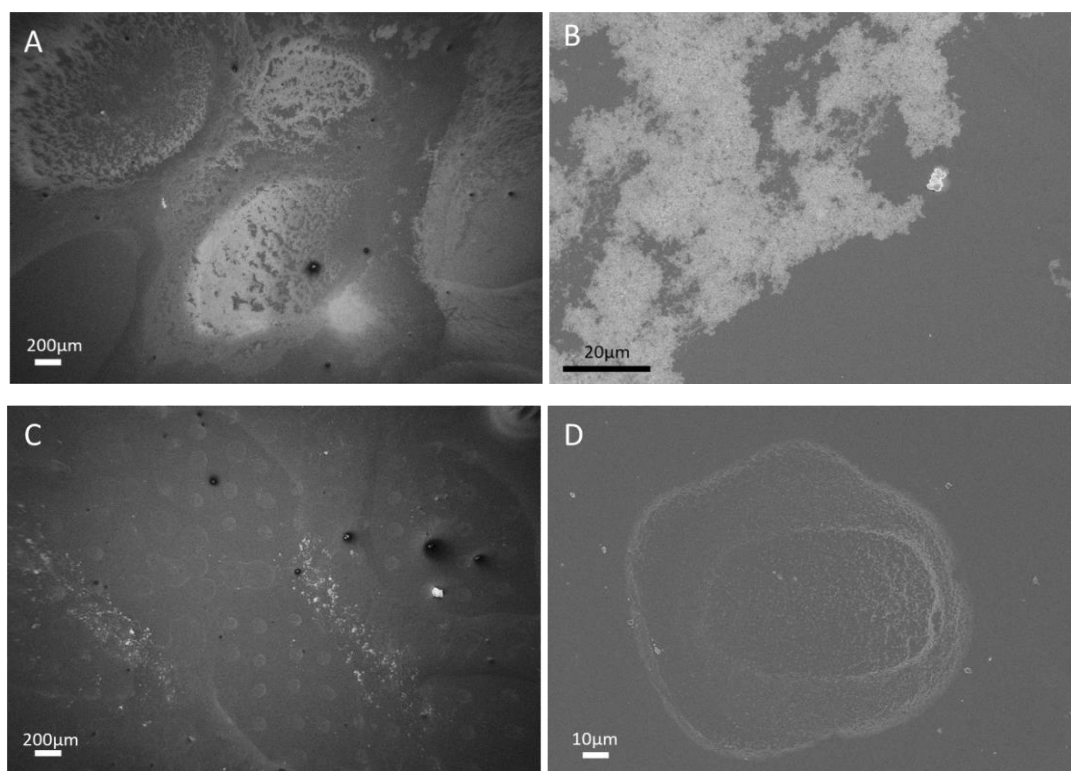
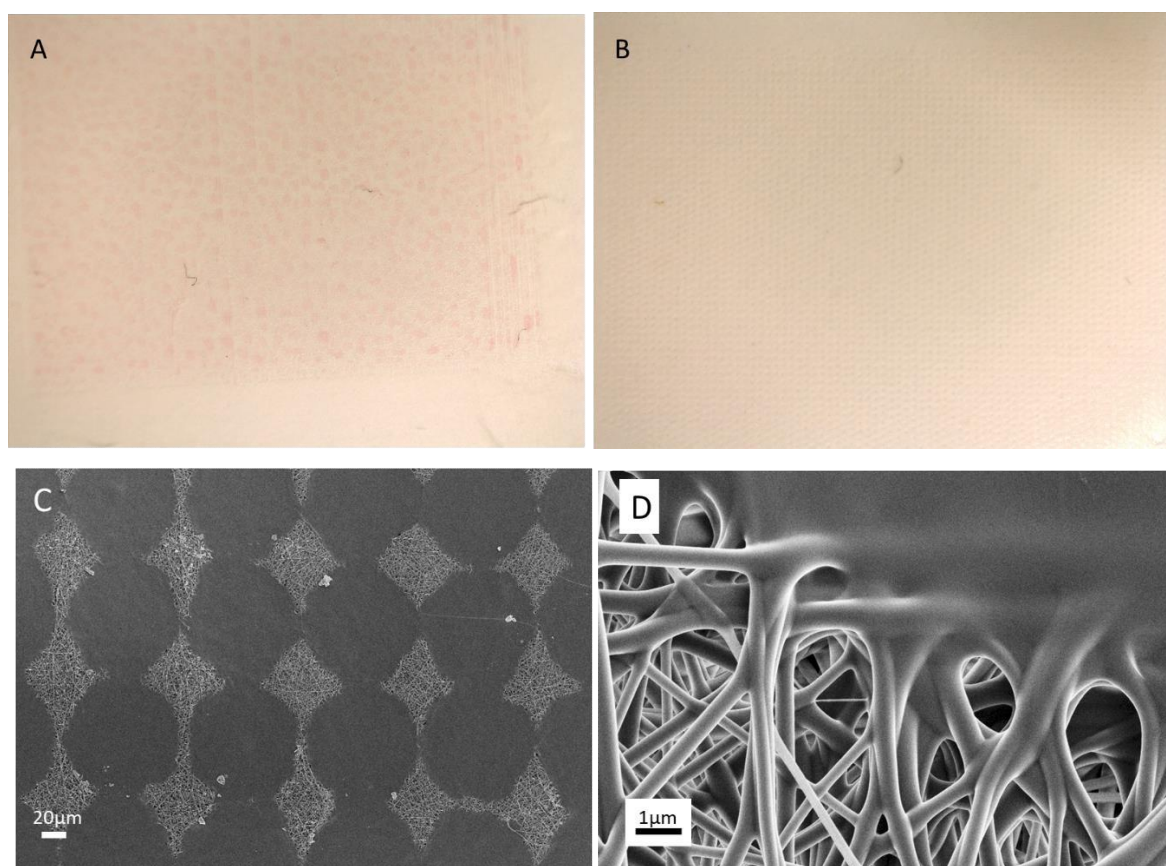


Figure 22. Scanning electron microscopy (SEM) images of inkjet printed samples with coloured ink on crosslinked solvent cast films/3D printed (SCBB) substrates printed with A-B) 450 dpi resolution and C-D) 100 dpi resolution (30× and 600× magnification).

The fibre substrates are more porous than the SCBB substrates meaning that they absorb the ink solution to a greater extent (as it was seen in the surface tension measurement in the section 6.4). The printed area on the non-crosslinked SCNF substrate with a resolution of 450 dpi could be seen with the naked eye, although the edges of the area were smudged (*Figure 23A*). The inkjet printing with a resolution of 100 dpi on non-crosslinked SCNF substrate had a sharper and well-defined pattern, where the individual droplets stayed separated from each other (*Figure 23B*). This was also observed on the SEM images where the ink solution dissolved the non-crosslinked fibrous surface layer completely (*Figure 23CD*).

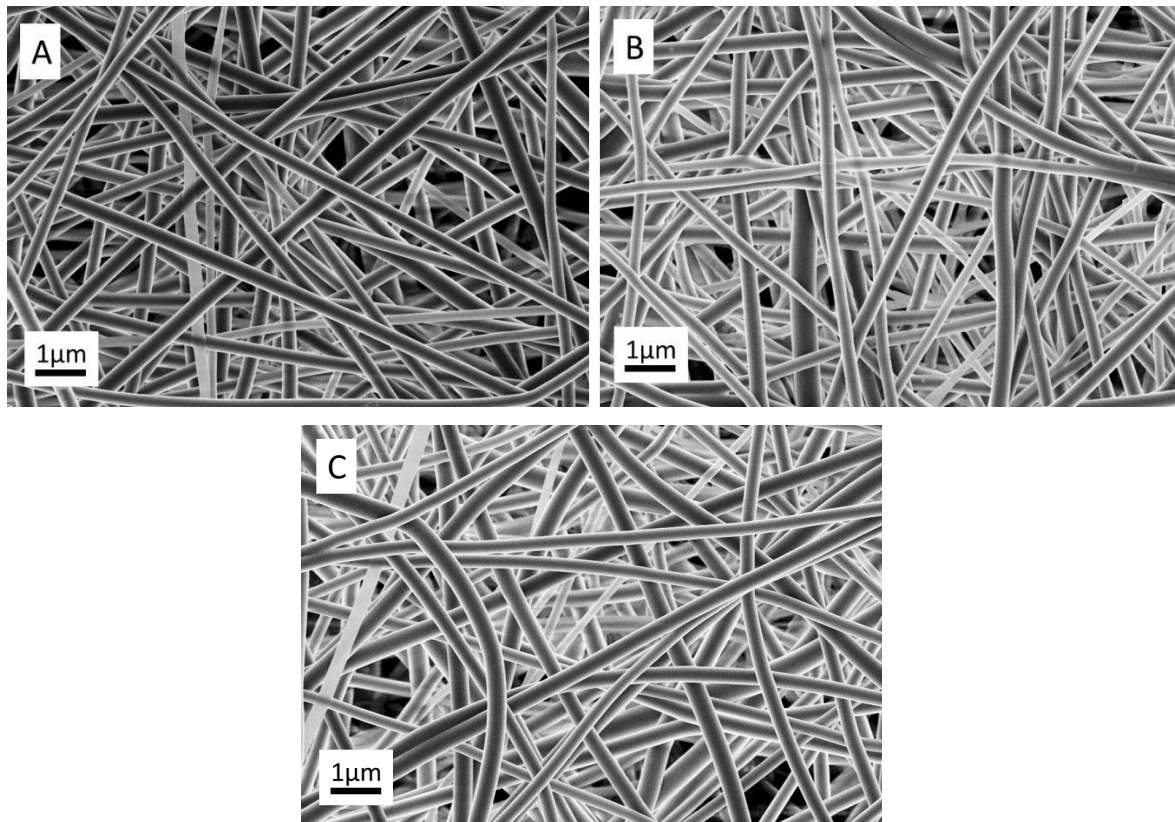


*Figure 23. A-B) Microscopy images of inkjet printed samples with coloured ink on non-crosslinked solvent cast/nanofibre (SCNF) substrates printed with A) 450 dpi resolution and B) 100 dpi resolution. C-D) Scanning electron microscopy (SEM) images of the printed samples on the non-crosslinked SCNF substrates printed with 100 dpi resolution at B) 250 $\times$  magnification and D) 10000 $\times$  magnification.*

The coloured ink was absorbed by the crosslinked fibres and the ink spread across the substrate. The printed area was not defined after the ink was printed on top of the SCNF substrate with a resolution of 450 dpi. On the other hand, the ink solution printed with a resolution of 100 dpi was not visible by naked eye, nor with SEM, as the droplets did not remain separate on the surface due to the absorption of the ink into the fibre layer. Thus, no apparent changes could be seen on the crosslinked fibres from the SEM images. The only



difference in the SEM images was a slightly white nuance of the fibres when comparing them to the images of the initial crosslinked fibres (*Figure 24*). It was suggested that the fibres absorbed all the ink very effectively and/or that the ink solution migrated straight through the fibre layer and settled along the SC film.



*Figure 24. A) Microscopy images of crosslinked solvent cast/nanofibre (SCNF) substrates B-C) of inkjet printed samples with coloured ink printed with B) 450 dpi resolution and C) 100 dpi resolution. (10000× magnification).*

## 7. Conclusions

Substrates from solvent casting, electrospinning and three-dimensional (3D) printing techniques were prepared. The solvent cast films served as a base for the bi-layered substrates with solvent cast film/nanofibre (SCNF) and solvent cast film/3D printed (SCBB) combinations. The substrates were crosslinked thermally for better stability in aqueous environment.

In conclusion, the mechanical strength of the substrates was not affected by the addition of the second layer in the bi-layered formulations nor the crosslinking. Interestingly, the crosslinking significantly changed the thickness of the SCNF substrates. Adhesion studies showed that crosslinking reduced the adhesive properties of all the substrates except for the 3D printed ones. The adhesion of the nanofibrous substrates was practically non-existent and would therefore cause minimal trauma to newly formed tissue upon removal of a wound dressing.

When comparing all the electrospun substrates from the stability study, the results from infrared spectra analysis revealed that the thermal crosslinking led to the biggest changes in the crystallinity. This crosslinking method seemed to render the most stable physical properties of the substrates over time, under both dry and wet conditions. In the solvent cast substrates, the degree of crystallinity increased slowly over time and the elevated humidity and temperature accelerated the crystallization process. The solvent cast substrates were crystalline already from the start. The thermal crosslinking seemed to stabilize the physical properties of the solvent cast substrates, which was also seen for the electrospun substrates. The results from the differential scanning calorimetry supported the findings from the spectral analysis, showing that the solvent cast films are stable regardless of the storage conditions or crosslinking. The melting temperature of the fibres varied more according to storage conditions and water uptake, but crosslinking stabilized also these substrates.

Although the solvent cast/3D printed substrates had an increased surface area with a macroporous surface structure, these are not suited for inkjet printing as the contact angle is heavily dependent on the location of the ink solution droplet. The addition of 40% propylene glycol to the ink solution lowered the contact angle for all substrates. Crosslinking lowered the contact angle even further for all substrates. The ink solution was absorbed evenly by the crosslinked solvent cast/nanofibre substrates and no clearly extinguishable printed droplet pattern was observed. However, these substrates showed the most promising

suitability for inkjet printing application, as the ink solution adhered well to the surface and/or solvent cast layer underneath.

Further studies could be focused on developing the bi-layered structure towards a multi-layer structure to combine the mechanical properties of the solvent cast films with the non-adhesiveness of the nanofibres also utilizing their suitability for inkjet printing. An additional top layer of electrospun fibres could be added to the multi-layered substrate to achieve non-adhesive properties. Eventually, suitable drug compound(s) such as antibiotics or analgesics could be introduced to the ink solution and/or other layers depending on the wanted release profile. The effect of the drug on the substrate properties and the drug release profile should then also be investigated. An analysis of the penetration abilities of the ink through addition of fluorescent compounds to the ink solution could be done to receive further information on the effects of inkjet printing. Furthermore, studies on the tissue-regenerative properties of the substrates in terms of cell growth and toxicity level of the materials in their combination and different formulations could be evaluated.

Stacking of multiple substrates creates composite dressings that combine the advantages of each layer. This results in wound dressings that provide more than one function in wound care management and, therefore, are more versatile. This work has provided some ideas on what types of substrates and methods that can be used in the development of the structure of new wound dressings.



## 8. Swedish summary (svensk sammanfattning)

Huden är kroppens största organ och har många olika funktioner att uppfylla. Årligen råkar miljontals människor ut för skador orsakade av flammor, hett vatten eller kokande olja. Dessa skador skapar lidande och kan leda till funktionshinder eller till och med dödsfall. Rapporter baserade på verkliga bevis har visat att det finns ett konstant behov av bättre sårförband eftersom både akuta och kroniska sår ökar i mängd årligen. Det finns en stor variation av sår och alla kräver olika terapeutiska tillvägagångssätt för att uppnå adekvat läkning. Detta ställer vissa krav på sårförbandens egenskaper och uppbyggnad.

Sårförband kan framställas av olika material. Traditionellt sett har man använt torra, vävda gasbindor gjorda av naturmaterial som t.ex. lin eller bomull. Sedan 1960-talet har sårförbandsprodukterna utvecklats i takt med att kunskaperna om sårvård ökat. Moderna sårförband har en aktiv roll i sårbehandlingsprocessen och bör erbjuda ett optimalt sårbehandlingsklimat genom att bibehålla fukt men avlägsna överskott av utsöndrad sårvätska. De måste även vara icke-allergiframkallande, giftfria, passa ihop med organiskt material, tillåta gasutbyte och erbjuda både mekaniskt skydd och isolering för såret. Utöver detta bör sårförbandet orsaka minimalt besvär för patienten och finnas tillgängliga till ett förmånligt pris. Aktiva bioföreningar som kitosan, elastin, alginat eller kollagen används ofta i moderna sårförband i kombination med syntetiska polymerer för att förbättra produktens mekaniska egenskaper. Eftersom kroppsdelarnas form varierar mycket, är flexibla sårförband med en icke-häftande yta mot såret att föredra. Den största utmaningen ligger i att hitta en beredningsform som klarar av att absorbera överflödiga vätskor som utsöndras från såret men samtidigt bibehåller en fuktig miljö och främjar snabb läkning utan att behöva bytas ut alltför ofta. Byte av sårförband alltför ofta kan bromsa upp läkningsprocessen eftersom ny vävnad lätt går sönder. Risken för detta måste ändå vägas mot att huden runtomkring såret kan ta skada av att utsättas för en alltför blöt miljö ifall det samlas för stora mängder utsöndrad sårvätska under förbandet. Dessa krav ställer höga krav på egenskaperna hos de material som används i sårförband. De bör ha goda mekaniska egenskaper och förmåga att svälla, dessutom bör de vara fysikalisk-kemiskt stabila. Utöver detta är det även möjligt att inkorporera farmaceutiskt aktiva komponenter så som antibiotika, analgetika, tillväxtfaktorer eller vitaminer i/på sårförbandet för att påskynda läkningsprocessen. Det finns olika metoder, t.ex. bläckstråleskrivning, som kan användas för att introducera tilläggskomponenter i sårförband.

De nuvarande tillvägagångssätten och de medicinska produkterna för sårhäkning är ofta otillräckliga för att uppnå en effektiv sårbehandling. Således finns det ett behov av avancerade sårvårdsprodukter såsom mer flexibla och interaktiva sårförband. Huvudsyftet med denna studie var att utveckla och undersöka nya polymerformuleringar och hur de lämpar sig för användning som biokompatibla och bioadhesiva sårförband.

I denna studie användes den bioaktiva föreningen natriumalginat (SA) i kombination med en syntetisk polymer, polyvinylalkohol (PVA), för att framställa enkel- och dubbelskiktade substrat för sårförband genom elektrospinning, filmgjutning, tredimensionell (3D) printteknik samt kombinationer av dessa. Både PVA och SA är vattenlösliga och blandades i ett 80:20 volymförhållande som hölls konstant för alla substrat. Den gjutna filmen fungerade som bas för de dubbelskiktade substraten. Tunna fibrer med en diameter av nanostorlek, applicerades på filmen genom elektrospinning. Elektrospunna fibrer har en exceptionellt stor yta eftersom fibrerna skapar en hålig väv. De är även mycket porösa vilket ökar upptaget och interaktionerna mellan fibrer och till exempel sårvätska. Den 3D-printade strukturen framställdes för att skapa ett stadigare substrat än fiberväven, med en lite porösare struktur än den gjutna filmen med hjälp av makroporer. Makroporerna bestod av ett printat mönster i form av en vaxkaka.

Det primära målet var att undersöka de fysikalisk-kemiska egenskaperna och stabiliteten under en månads tid hos de framställda substraten. För detta användes infraröd spektroskopi samt differentiell svepkalorimetrisk analys. Även substratens sönderfall i våta kroppsvätskeliknande förhållanden undersöktes genom att förvara dem i fosfatbuffrad saltlösning i 37 °C under 7 dagar. Substratens ytegenskaper, relaterade till substratens häftningsförmåga på huden, utreddes med hjälp av ett adhesionstest och de mekaniska egenskaperna med ett punkteringstest. Utöver detta utvärderades substratens lämplighet för att ytbehandlas med bläckstråleutskrift av vattenbaserat bläck med aktiva föreningar. Här utnyttjades bilder från svepelektronmikroskop (SEM) för att visualisera bläckets spridning på ytan. SEM-bilder användes även för att undersöka strukturen hos substraten i sönderfallsstudien. Kontaktvinkelmätningar användes för att mäta interaktionerna mellan bläck och substrat.

Substraten värmebehandlades så att fysikaliska tvärbindingar uppstod i substratens struktur för att förbättra deras stabilitet i en vattenhaltig miljö. Resultatet från adhesionsstudier visade att tvärbinding minskade adhesionsegenskaperna hos alla substraten förutom hos de 3D-printade. Vidhäftningen av fibersubstraten till ett artificiellt hudmembran var praktiskt

taget obefintlig och skulle därför troligtvis orsaka minimal skada på nybildad vävnad vid avlägsnande av sårförband. Filmerna visade sig vara mekaniskt starkast i punkteringstestet. Vid jämförelse av fibersubstraten från stabilitetsstudien, visade resultaten från infrarödspektraanalysen att den fysikaliska tvärbindingen ledde till de största förändringarna i substratens kristallinitet. Denna tvärbindningsmetod verkade ge de mest stabila fysikaliska egenskaperna hos substraten under en månads lagringstid i både torra (rumstemperatur, 0 % relativ luftfuktighet) och våta (40 °C, 75 % relativ luftfuktighet) förhållanden. Graden av kristallinitet ökade gradvis under stabilitetsstudien och den förhöjda fuktigheten och temperaturen accelererade kristalliseringsprocessen. De gjutna polymerfilmerna uppvisade kristallina egenskaper redan från början. Värmebehandlingen verkade stabilisera de fysikaliska egenskaperna hos både de gjutna filmerna och fibersubstraten. Infrarödspektroskopi och differentiell svepkalorimetri visade att de gjutna filmerna var de mest stabila substraten efter en lagringsperiod på en månad. Resultaten från differentialsvepkalorimetern stödde resultaten från spektralanalysen, vilket visade att de gjutna filmerna är stabila oberoende av lagringsbetingelser eller tvärbinding. Fibernas smälttemperatur varierade mer än för de lösningsmedelsgjutna substraten, i enlighet med lagringsförhållanden och vattenupptagning, men värmebehandlingen stabiliserade även dessa substrat. Även om de filmgjutna/3D-tryckta substraten hade en ökad ytareal tack vare sin makroporösa ytstruktur, är dessa inte lämpade för bläckstråleskrivning eftersom kontaktvinkeln är starkt beroende av positionen där bläcklösningens droppen landar. Tillsatsen av propylenglykol (40 %) till bläcklösningen sänkte kontaktvinkeln för alla substrat. Värmebehandlingen sänkte kontaktvinkeln ytterligare för alla substrat. Bläcklösningen absorberades jämnt av de tvärbundna filmgjutna/nanofiber-substraten och inget klart urskiljbart droppmönster kunde observeras. Dessa substrat visade emellertid den mest lovande lämpligheten för bläckstråleskrivning då bläcklösningen fästes väl vid ytan och/eller filmskiktet under fibrerna.

Inom framtida studier kunde man rikta in sig på att utveckla den dubbelskiktade strukturen mot en flerskiktsstruktur för att kombinera de mekaniska egenskaperna hos de gjutna filmerna med fibrernas låga vidhäftningsförmåga i flera lager. Detta utnyttjar också fibrernas lämplighet för bläckstråleskrivning. Eventuella läkemedelsföreningar, såsom antibiotika eller analgetika, kunde tillsättas i bläcklösningen eller inkorporeras i de andra skikten beroende på den önskade frisättningsprofilen. Interaktionerna mellan läkemedlet och substraten samt läkemedelsfrigöringsprofilen bör i så fall även undersökas. Det kunde även

görs en analys av bläckets penetreringsförmåga genom att tillsätta fluorescerande föreningar till bläcklösningen för att få ytterligare information om bläckstråleskrivningens effekter på substraten. Vidarestudier på substratens vävnadsregenerativa egenskaper (effekt på celltillväxt och toxicitetsnivå) för SA och PVA i de olika substraten borde utföras. Staplandet av flera substrat på varandra skapar ett kompositförband som kombinerar fördelarna med varje lager. Detta resulterar i ett sårförband som besitter mer än en funktion inom sårvårdshandlingen och som därför kan användas på ett mer mångsidigt sätt. Detta arbete bidragit med idéer om vilka typer av substrat och metoder som kan användas vid utvecklingen av strukturen och egenskaper hos nya (komposit)sårförband.

## 9. References

- [1] P. C. Smith, M. Cáceres, C. Martínez, A. Oyarzún, and J. Martínez, “Gingival wound healing: an essential response disturbed by aging?,” *J. Dent. Res.*, vol. 94, no. 3, pp. 395–402, 2015.
- [2] P. Zahedi, I. Rezaeian, S. O. Ranaei-Siadat, S. H. Jafari, and P. Supaphol, “A review on wound dressings with an emphasis on electrospun nanofibrous polymeric bandages,” *Polym. Adv. Technol.*, vol. 21, no. 2, pp. 77–95, 2010.
- [3] J. S. Boateng, K. H. Matthews, H. N. E. Stevens, and G. M. Eccleston, “Wound Healing Dressings and Drug Delivery Systems: A Review,” *J. Pharm. Sci.*, vol. 97, no. 8, pp. 2892–2923, 2008.
- [4] V. Jones, J. Grey, and K. Harding, “ABC of wound healing: Wound dressings,” *Br. Med. J.*, vol. 332, no. April, pp. 777–780, 2006.
- [5] W. Paul and C. Sharma, “Chitosan and alginate wound dressings: a short review,” *Trends Biomater Artif Organs*, vol. 18, no. 1, pp. 18–23, 2004.
- [6] H. Ç. Arca and S. Şenel, “Chitosan based systems for tissue engineering part 1: hard tissues,” *FABAD J. Pharm. Sci.*, vol. 33, no. December 2008, pp. 35–49, 2008.
- [7] J. F. Guest, K. Vowden, and P. Vowden, “The health economic burden that acute and chronic wounds impose on an average clinical commissioning group/health board in the UK,” *J. Wound Care*, vol. 26, no. 6, pp. 292–303, 2017.
- [8] “Skin Structure,” *WebMD*, 2018. [Online]. Available: <https://www.webmd.com/skin-problems-and-treatments/ss/slideshow-skin-infections>. [Accessed: 21-May-2018].
- [9] E. A. Kamoun, X. Chen, M. S. Mohy Eldin, and E. R. S. Kenawy, “Crosslinked poly(vinyl alcohol) hydrogels for wound dressing applications: A review of remarkably blended polymers,” *Arab. J. Chem.*, vol. 8, no. 1, pp. 1–14, 2015.
- [10] J. P. E. Junker, R. A. Kamel, E. J. Catterson, and E. Eriksson, “Clinical Impact Upon Wound Healing and Inflammation in Moist, Wet, and Dry Environments,” *Adv. Wound Care*, vol. 2, no. 7, pp. 348–356, 2013.
- [11] K. T. Shalumon, K. H. Anulekha, S. V. Nair, S. V. Nair, K. P. Chennazhi, and R. Jayakumar, “Sodium alginate/poly(vinyl alcohol)/nano ZnO composite nanofibers for antibacterial wound dressings,” *Int. J. Biol. Macromol.*, vol. 49, no. 3, pp. 247–

- 254, 2011.
- [12] J. O. Kim *et al.*, “Development of polyvinyl alcohol–sodium alginate gel-matrix-based wound dressing system containing nitrofurazone,” *Int. J. Pharm.*, vol. 359, no. 1–2, pp. 79–86, Jul. 2008.
- [13] N. Gomathi, A. Sureshkumar, and S. Neogi, “RF plasma-treated polymers for biomedical applications,” *Curr. Sci.*, vol. 94, no. 11, pp. 1478–1486, 2008.
- [14] A. S. Hoffman, “Hydrogels for biomedical applications,” *Adv. Drug Deliv. Rev.*, vol. 64, pp. 18–23, Dec. 2012.
- [15] M. . Hans and A. . Lowman, “Biodegradable nanoparticles for drug delivery and targeting,” *Curr. Opin. Solid State Mater. Sci.*, vol. 6, no. 4, pp. 319–327, Aug. 2002.
- [16] C. . DeMerlis and D. . Schoneker, “Review of the oral toxicity of polyvinyl alcohol (PVA),” *Food Chem. Toxicol.*, vol. 41, no. 3, pp. 319–326, 2003.
- [17] Y. Qiu and K. Park, “Environment-sensitive hydrogels for drug delivery,” *Adv. Drug Deliv. Rev.*, vol. 53, no. 3, pp. 321–339, Dec. 2001.
- [18] B. Bolto, T. Tran, M. Hoang, and Z. Xie, “Crosslinked poly(vinyl alcohol) membranes,” *Prog. Polym. Sci.*, vol. 34, no. 9, pp. 969–981, Sep. 2009.
- [19] M. Kokabi, M. Sirousazar, and Z. M. Hassan, “PVA–clay nanocomposite hydrogels for wound dressing,” *Eur. Polym. J.*, vol. 43, no. 3, pp. 773–781, Mar. 2007.
- [20] M.-R. Hwang *et al.*, “Gentamicin-Loaded Wound Dressing With Polyvinyl Alcohol/Dextran Hydrogel: Gel Characterization and In Vivo Healing Evaluation,” *AAPS PharmSciTech*, vol. 11, no. 3, pp. 1092–1103, 2010.
- [21] R. Jayakumar, M. Prabakaran, P. T. Sudheesh Kumar, S. V. Nair, and H. Tamura, “Biomaterials based on chitin and chitosan in wound dressing applications,” *Biotechnol. Adv.*, vol. 29, no. 3, pp. 322–337, May 2011.
- [22] A. F. Martins, P. V. A. Bueno, E. A. M. S. Almeida, F. H. A. Rodrigues, A. F. Rubira, and E. C. Muniz, “Characterization of N-trimethyl chitosan/alginate complexes and curcumin release,” *Int. J. Biol. Macromol.*, vol. 57, pp. 174–184, Jun. 2013.
- [23] D. M. Panaitescu, A. N. Frone, M. Ghiurea, and I. Chiulan, “Influence of storage conditions on starch/PVA films containing cellulose nanofibers,” *Ind. Crops Prod.*, vol. 70, pp. 170–177, Aug. 2015.

- [24] H. H. Tønnesen and J. Karlsen, “Alginate in drug delivery systems,” *Drug Dev. Ind. Pharm.*, vol. 28, no. 6, pp. 621–630, 2002.
- [25] X. Wang, B. Ding, G. Sun, M. Wang, and J. Yu, “Electro-spinning/netting: A strategy for the fabrication of three-dimensional polymer nano-fiber/nets,” *Prog. Mater. Sci.*, vol. 58, no. 8, pp. 1173–1243, 2013.
- [26] R. Jaeger, M. M. Bergshoeff, C. M. I. Batlle, H. Schönherr, and G. Julius Vancso, “Electrospinning of ultra-thin polymer fibers,” *Macromol. Symp.*, vol. 127, no. 1, pp. 141–150, Feb. 1998.
- [27] M. Ziabari, V. Mottaghitalab, and A. K. Haghi, “Evaluation of electrospun nanofiber pore structure parameters,” *Korean J. Chem. Eng.*, vol. 25, no. 4, pp. 923–932, 2008.
- [28] S. Agarwal, J. H. Wendorff, and A. Greiner, “Use of electrospinning technique for biomedical applications,” *Polymer (Guildf.)*, vol. 49, no. 26, pp. 5603–5621, 2008.
- [29] N. Zander, “Hierarchically Structured Electrospun Fibers,” *Polymers (Basel)*, vol. 5, no. 1, pp. 19–44, Jan. 2013.
- [30] K. E. Park, S. Y. Jung, S. J. Lee, B.-M. Min, and W. H. Park, “Biomimetic nanofibrous scaffolds: Preparation and characterization of chitin/silk fibroin blend nanofibers,” *Int. J. Biol. Macromol.*, vol. 38, pp. 165–173, 2006.
- [31] I. Rezaeian, B. Motealleh, M. Gholami, P. Zahedi, A. Salehpour, and M. A. Zarandi, “Drug release, cell adhesion and wound healing evaluations of electrospun carboxymethyl chitosan/polyethylene oxide nanofibres containing phenytoin sodium and vitamin C,” *IET Nanobiotechnology*, vol. 9, no. 4, pp. 191–200, 2015.
- [32] N. Bhardwaj and S. C. Kundu, “Electrospinning: A fascinating fiber fabrication technique,” *Biotechnol. Adv.*, vol. 28, no. 3, pp. 325–347, 2010.
- [33] S. Safi, M. Morshed, S. A. Hosseini Ravandi, and M. Ghiaci, “Study of Electrospinning of Sodium Alginate , Blended Solutions of Sodium Alginate / Poly ( vinyl alcohol ) and Sodium Alginate / Poly ( ethylene oxide ),” *J Appl Polym Sci*, vol. 104, pp. 3245–3255, 2007.
- [34] M. Preis, K. Knop, and J. Breitzkreutz, “Mechanical strength test for orodispersible and buccal films,” *Int. J. Pharm.*, vol. 461, pp. 22–29, 2014.
- [35] A. B. M. Buanz, C. C. Belaunde, N. Soutari, C. Tuleu, O. Gul, and S. Gaisford, “Ink-

- jet printing versus solvent casting to prepare oral films: Effect on mechanical properties and physical stability,” *Int. J. Pharm.*, vol. 494, pp. 611–618, 2015.
- [36] J. C. Visser *et al.*, “Orodispersible films in individualized pharmacotherapy: The development of a formulation for pharmacy preparations,” *Int. J. Pharm.*, vol. 478, pp. 155–163, 2015.
- [37] V. Garsuch and J. Breitzkreutz, “Comparative investigations on different polymers for the preparation of fast-dissolving oral films.,” *J. Pharm. Pharmacol.*, vol. 62, no. 4, pp. 539–45, 2010.
- [38] C. L. Ventola, “Medical Applications for 3D Printing: Current and Projected Uses,” *Pharm. Ther.*, vol. 39, no. 10, pp. 704–711, 2014.
- [39] G. F. Acosta-Vélez and B. M. Wu, “3D Pharming : Direct Printing of Personalized Pharmaceutical Tablets Abstract Powder Bed Inkjet 3D Printing,” *Polym. Sciences*, vol. 1, no. 2, pp. 1–10, 2016.
- [40] J. Goole and K. Amighi, “3D printing in pharmaceuticals: A new tool for designing customized drug delivery systems,” *Int. J. Pharm.*, vol. 499, pp. 376–394, 2016.
- [41] N. Sandler and M. Preis, “Printed Drug-Delivery Systems for Improved Patient Treatment,” *Trends Pharmacol. Sci.*, vol. 37, no. 12, pp. 1070–1080, 2016.
- [42] N. Scoutaris, S. Ross, and D. Douroumis, “Current Trends on Medical and Pharmaceutical Applications of Inkjet Printing Technology,” *Pharm. Res.*, vol. 33, no. 8, pp. 1799–1816, Aug. 2016.
- [43] L. Wang, S. T. Beyer, Q. C. Cronk, and K. Walus, “Delivering high-resolution landmarks using inkjet micropatterning for spatial monitoring of leaf expansion.,” *Plant Methods*, vol. 7, no. 1, p. 1, Jan. 2011.
- [44] B. Derby, “Inkjet Printing of Functional and Structural Materials: Fluid Property Requirements, Feature Stability, and Resolution,” *Annu. Rev. Mater. Res.*, vol. 40, pp. 395–414, 2010.
- [45] C.-H. Lin, H. Yang, F.-Y. Chang, S.-H. Chang, and M.-T. Yen, “Fast patterning microstructures using inkjet printing conformal masks,” *Microsyst. Technol.*, vol. 14, no. 9–11, pp. 1263–1267, Oct. 2008.
- [46] M. J. J. Coenen, T. M. W. L. Slaats, T. M. Eggenhuisen, and P. Groen, “Inkjet printing



- the three organic functional layers of two-colored organic light emitting diodes,” *Thin Solid Films*, vol. 583, pp. 194–200, 2015.
- [47] B. Derby, “Additive Manufacture of Ceramics Components by Inkjet Printing,” *Engineering*, vol. 1, no. 1, pp. 113–123, 2015.
- [48] L. Setti, A. Fraleoni-Morgera, B. Ballarin, A. Filippini, D. Frascaro, and C. Piana, “An amperometric glucose biosensor prototype fabricated by thermal inkjet printing,” *Biosens. Bioelectron.*, vol. 20, no. 10, pp. 2019–2026, 2005.
- [49] W. Zhu, X. Ma, M. Gou, D. Mei, K. Zhang, and S. Chen, “3D printing of functional biomaterials for tissue engineering,” *Curr. Opin. Biotechnol.*, vol. 40, pp. 103–112, 2016.
- [50] H. C.-J. Huang K-T, Fang Y-L, Hsieh P-S, Lee C-C, Dai N-T, “Zwitterionic Nanocomposite Hydrogels as,” *J. Mater. Chem. B*, vol. 4, pp. 4206–4215, 2016.
- [51] European Medicines Agency, “Guideline On Stability Testing: Stability Testing Of Existing Active Substances And Related Finished Products.” p. rev 1 corr, CPMP/QWP/122/02, 2003.
- [52] M. Miraftab, A. N. Saifullah, and A. Çay, “Physical stabilisation of electrospun poly(vinyl alcohol) nanofibres: comparative study on methanol and heat-based crosslinking,” *J. Mater. Sci.*, vol. 50, no. 4, pp. 1943–1957, Feb. 2015.
- [53] I. Tamm *et al.*, “Development of Suberin Fatty Acids and Chloramphenicol-Loaded Antimicrobial Electrospun Nanofibrous Mats Intended for Wound Therapy,” *J. Pharm. Sci.*, vol. 105, no. 3, pp. 1239–1247, 2016.
- [54] H. Wickström *et al.*, “Inkjet printing of drug-loaded mesoporous silica nanoparticles—a platform for drug development,” *Molecules*, vol. 22, no. 11, pp. 1–20, 2017.
- [55] C. Birck, S. Degoutin, N. Tabary, V. Miri, and M. Bacquet, “New crosslinked cast films based on poly(vinyl alcohol): Preparation and physico-chemical properties,” *Express Polym. Lett.*, vol. 8, no. 12, pp. 941–952, 2014.
- [56] G. R. Hansen Eric F., Derrick Michele R., Schilling Michael R., “The Effects of Solution Application on Some Mechanical and Physical Properties of Thermoplastic Amorphous Polymers Used in Conservation: Poly(vinyl acetate)s,” *J. Am. Inst. Conserv.*, vol. 30, no. 2, pp. 203–213, 1991.

- [57] S. El-Sayed, K. H. Mahmoud, A. A. Fatah, and A. Hassen, “DSC, TGA and dielectric properties of carboxymethyl cellulose/polyvinyl alcohol blends,” *Phys. B Condens. Matter*, vol. 406, no. 21, pp. 4068–4076, Nov. 2011.
- [58] S. K. Mallapragada and N. a Peppas, “Dissolution Mechanism of Semicrystalline Poly ( vinyl alcohol) in Water,” *J. Polym. Sci.*, vol. 34, no. 7, pp. 1339–1346, 1996.
- [59] J. P. Soares, J. E. Santos, G. O. Chierice, and E. T. G. Cavalheiro, “Thermal behavior of alginic acid and its sodium salt,” *Eclética Química*, vol. 29, no. 2, pp. 57–64, 2004.
- [60] M. S. Islam and M. R. Karim, “Fabrication and characterization of poly(vinyl alcohol)/alginate blend nanofibers by electrospinning method,” *Colloids Surfaces A Physicochem. Eng. Asp.*, vol. 366, pp. 135–140, 2010.
- [61] G. Lawrie *et al.*, “Interactions between Alginate and Chitosan Biopolymers Characterized Using FTIR and XPS,” *Biomacromolecules*, vol. 8, no. 8, pp. 2533–2541, 2007.
- [62] H. S. Mansur, C. M. Sadahira, A. N. Souza, and A. A. P. Mansur, “FTIR spectroscopy characterization of poly (vinyl alcohol) hydrogel with different hydrolysis degree and chemically crosslinked with glutaraldehyde,” *Mater. Sci. Eng. C*, vol. 28, no. 4, pp. 539–548, May 2008.
- [63] J. W. C. Matos-Pérez, J. White, “Polymer Composition and Substrate Influences on the Adhesive Bonding of a Biomimetic, Cross-Linking Polymer,” *J Am Chem Soc.*, vol. 134, no. 22, pp. 9498–9505, 2013.
- [64] S. Singh, S. Jain, M. S. Muthu, S. Tiwari, and R. Tilak, “Preparation and Evaluation of Buccal Bioadhesive Films Containing Clotrimazole,” *AAPS PharmSciTech*, vol. 9, no. 2, pp. 660–667, 2008.
- [65] M. Palo *et al.*, “Development of Oromucosal Dosage Forms by Combining Electrospinning and Inkjet Printing,” *Mol. Pharm.*, vol. 14, no. 3, pp. 808–820, 2017.
- [66] FUJIFILM Dimatix Inc., “Product Data: Spectra SL-128 AA Rev. 08.” Tokyo, Japan, 2015.
- [67] D. Jang, D. Kim, and J. Moon, “Influence of fluid physical properties on ink-jet printability,” *Langmuir*, vol. 25, no. 5, pp. 2629–2635, 2009.